UCRL 9601

UNIVERSITY OF CALIFORNIA

Ernest O. Lawrence

Radiation Laboratory

EXPERIMENTAL STUDY OF HYDROMAGNETIC WAVES IN PLASMA

BERKELEY, CALIFORNIA

DISCLAIMER

UCRL-9601

UNIVERSITY OF CALIFORNIA

Lawrence Radiation Laboratory
Berkeley, California

Contract No. W-7405-eng-48

EXPERIMENTAL STUDY OF HYDROMAGNETIC WAVES IN PLASMA

Alan W. DeSilva

(Ph. D. Thesis)

March 17, 1961

Printed in USA. Price $2.25. Available from the
Office of Technical Services
U. S. Department of Commerce
Washington 25, D.C.

EXPERIMENTAL STUDY OF HYDROMAGNETIC WAVES IN PLASMA

Contents

EXPERIMENTAL STUDY OF HYDROMAGNETIC WAVES IN PLASMA

Alan W. DeSilva

Lawrence Radiation Laboratory
University of California
Berkeley, California

March 17, 1961

ABSTRACT

An experiment is decribed in which a torsional hydromagnetic wave is excited in a cylindrical hydrogen plasma. The theory of the waves is briefly described and expressions are derived for the wave velocity, attenuation, field distributions, and the tube input impedance. Measurements are presented which verify the linear dependence of wave velocity on magnetic field and show fairly good agreement with theory for variation of mass density. The temperature of the plasma is determined experimentally by a direct resistivity measurement, and is found to agree well with the observed temperature derived from wave damping. The variation of attenuation constant with magnetic field is shown to be consistent with theory. Reflections of the waves occurring from insulating and conducting boundaries, and from a plasma-neutral gas interface are described. In all cases the phase changes at reflection are in agreement with theory. The radial magnetic field distributions have been experimentally investigated and compared to theoretical predictions based on a modal analysis of the driving pulse. A description is given of the plasma preparation process and of measurements of the plasma properties, which show that the plasma is $>85\%$ ionized with an ion density $>5\times10^{15}$ cm^{-3} and has a temperature of about 12,000 ^{o}K.

I. INTRODUCTION

Hydromagnetic waves were first described in 1942 by Hannes Alfvén,[1] who suggested that waves of this sort might account for the existence of sunspots. His work was followed up by treatments of these waves by Walén,[2] Astrom,[3] and Herlofson.[4] Since then, a rather extensive literature on the subject has accumulated (see Bibliography). Comparatively little, however, has been done in the way of experimental work. The reasons for this are found in the considerations of Lundquist,[5] who showed that for laboratory-size experiments with practical magnetic fields, one needed fluids with very high electrical conductivities to obtain waves that would not be highly damped. The liquid metals mercury and sodium offered the best possibilities for experiment, and accordingly experiments were performed by Lundquist[5] and Lehnert[6] using these metals. A wave motion was detected, but the damping was very high, as predicted.

With the rapid development of the technology of plasma physics, it became possible to perform hydromagnetic wave experiments in ionized gases. The attenuation coefficient for the waves is inversely proportional to the wave velocity, so, even though electrical conductivities of practical plasmas are low, the greatly increased wave velocity over that in liquid metals means that in a plasma dissipation will also be low, making it an attractive medium for wave experiments. Observations of such waves in a plasma were first reported by Bostick and Levine in 1952.[7] Reports of the experimental generation of hydromagnetic waves were made almost simultaneously in 1959 by Allen et al.[8] and by Jephcott.[9] The work reported in this paper is an attempt to establish quantitative correspondence between hydromagnetic wave theory and experiment.[10]

A hydromagnetic wave is the result of interactions between a moving, electrically conducting fluid and an externally imposed static magnetic field. Motions of the fluid in the field induce electrical currents, and reaction forces from these currents oppose the original motion.

Simultaneously, energy is stored in the perturbation magnetic fields. When these fields collapse currents are induced; the forces due to these currents tend to restore the fluid to its original condition. These are the elements of a wave motion--a continuum that has restoring forces that tend to oppose displacements.

An intuitive description of the transverse hydromagnetic wave was given by Alfvén in an analogy with waves on a stretched string.[1] The transverse wave resulting from plucking a string travels with a velocity given by the square root of the tension divided by the linear mass density. Now it is well known that the "lines of force" of a magnetic field behave as though there were a tension along the lines of B^2/μ_0 newtons/meter^2, along with a hydrostatic pressure of $B^2/2\mu_0$ newtons/meter^2. Since a hydrostatic pressure does not affect the wave motion, we consider only the tension. If there is an electrically conducting fluid in the field, the fluid particles act as though they were bound tightly to the field lines. This may be easily seen by imagining such a fluid element to be suddenly displaced toward a region of different magnetic field strength. Consider a path around the fluid element enclosing some magnetic flux: this flux cannot change, for if it did, an electric field would be set up around the path according to Faraday's law. But since the fluid is a good conductor, a current flows just sufficient to ensure that the flux remains constant. Saying the flux is constant through any fluid element is equivalent to saying that the fluid particles are attached to the field lines. By analogy with the string then, we can imagine transverse waves traveling with a velocity given by the square root of the tension per unit area, divided by the linear mass density per unit area: $V = B/\sqrt{\mu_0 \rho}$. This is the Alfvén velocity, and can be shown by rigorous analysis to be the characteristic speed of a transverse hydromagnetic wave.

The experiments of Lehnert serve to illustrate simply the generation of hydromagnetic waves, and provide a good introduction to this experiment, which is basically very similar.[6] A cylindrical vessel was provided with a sort of false bottom in the form of a disc

that could be rotated from the outside about the cylinder axis. When the vessel was filled with liquid sodium, the whole apparatus was placed in an axial magnetic field of about 10 kgauss. The magnetic field lines penetrated the fluid, and provided the necessary stiffness for a wave motion to exist. The disc at the bottom was now oscillated about its axis at frequency of 30 cps. The fluid immediately above the plate was set in motion and a torsional wave induced that propagated to the top surface of the liquid. The wave was observed by measuring with a probe the radial electric field produced at the top surface of the fluid.

The experiment reported in this paper is conceptually very similar. In this case, the cylinder was filled with a plasma of ionized hydrogen (see Fig. 1) and the torsional oscillation excited by a radial current flow at one end, driven from an external circuit. For electric fields perpendicular to the static magnetic field a plasma behaves like a material with a high dielectric constant. Hence the cylinder may alternatively be considered as a dielectric-filled waveguide. Measurements have been made of wave velocity, attenuation, impedance, field distributions, and reflections.

We shall first develop the theory needed for a comparison with the results of experiment.

A. Definitions of Symbols

A_n, B_n, C_n	Defined in Eq. (2.21).
B_0	Static axial magnetic field of induction.
D	Defined above Eq. (2.22).
E	Electric field strength.
F	Defined following Eq. (2.18).
I	Unit dyad.
J_n	Bessel Function of nth order.

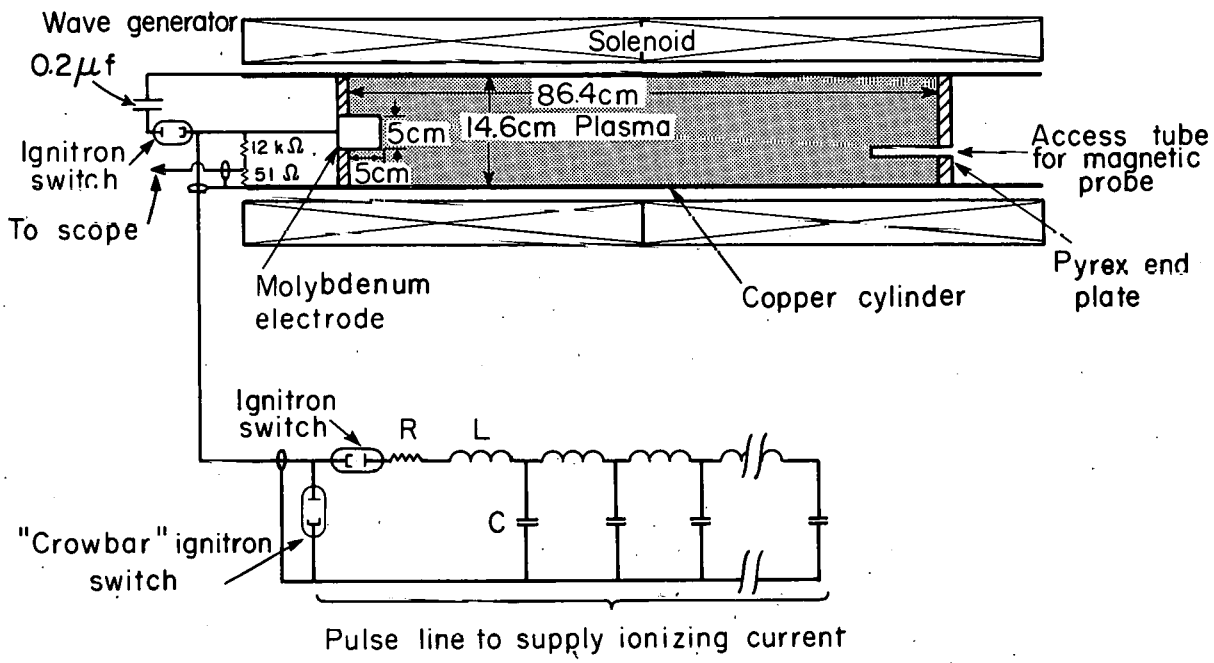

Fig. 1. Schematic diagram of experimental equipment.

κ Coefficient of thermal conductivity.

L Damping length (distance in which wave field attenuates to 1/e of its initial value).

N_n Neumann function of nth order.

P^{jk} Momentum transferred in unit time in unit volume from kth particle species to jth particle species.

Q Quality factor for radial diffusion. See Eq. (3.5).

S Scalar operator = $\frac{1}{r}\frac{\partial}{dr}\left(r\frac{\partial}{\partial r}\right) - \frac{1}{r^2}$.

T Temperature

U Velocity of ionizing wave.

V Complex Alfvén velocity $\left(\frac{B_0}{\sqrt{\mu_0\rho_1}} = \frac{B_0}{\sqrt{\mu_0\rho_0}}\frac{1}{\sqrt{1+i\xi}}\right)$.

V_s Sound velocity.

Z_0 Input impedance to waveguide.

$a_\perp$ $\frac{b_\perp}{\sqrt{\mu_0\rho_0}}$ Where $b_\perp$ is the θ field due to ionizing current flow.

a radius of central electrode.

b radius of tube.

c. assumed inner radius of outer electrode (Fig. 3).

$b_{r,\theta,z}$ Perturbation magnetic field of induction associated with wave.

C Velocity of light.

e Unit electrical charge.

e_i Ionization energy per unit mass.

e_d Dissociation energy per unit mass.

j Current density.

k Real part of propagation constant (see Eq. 2.29).

k_{cn} Radial wave number (defined above Eq. (2.59) — see also Eq.(2.20).

ℓ Length of hydromagnetic waveguide.

m_j Mass of particle of type j.

n_j Number density of particles of type j.

p Complex propagation constant (see Eq. (2.29).

p_j Partial pressure of jth particle species.

v_j Average velocity of particles of type j.

v_2 Axial velocity of gas behind ionizing wavefront.

$\hat{z}$ Unit vector in direction of static magnetic field.

α Defined above Eq. (2.15).

β $\omega^2/(V^2 k_c^2)$.

γ Proportionality factor between p^{ni} and $v_i - v_n$. See definition above Eq. (2.12).

ϵ Attenuation constant. See Eq. (2.29).

η Resistivity tensor = $\eta_{\parallel} \hat{z}\hat{z} + \eta_{\perp} (I - \hat{z}\hat{z})$

μ_0 Permeability of free space = $(4\pi \times 10^{-7}$ Henrys/meter).

ν_{ni} Collision frequency for a neutral particle with ions.

ξ $\frac{\omega}{\nu_{ni}} \frac{\rho_n}{\rho_0}$

ρ Mass density of a gas component. (Subscripts are: n = neutrals; i = ions; e = electrons; o = total mass density; 1 = complex density as defined following Eq. (2.12).

τ Coupling constant for ions and neutral particles. See Eq. (A.4).

σ_{ni} Charge exchange cross section.

ω Angular frequency of wave.

ω_{ce} Electron cyclotron angular frequency = $\frac{eB_0}{m_e}$.

ω_{ci} Ion cyclotron angular frequency = $\frac{eB_0}{m_i}$.

Ω $\frac{\omega}{\omega_{ci}} \frac{\rho_1}{nm_i}$

$\Im$ Defined following Eq. (2.62).

II. THEORY OF AXISYMMETRIC WAVES IN A CYLINDRICAL PLASMA

A. Basic Equations

We shall describe some of the types of hydromagnetic waves that can exist in a cylindrical plasma imbedded in a uniform axial magnetic field. Previous treatments of this problem are reviewed in Appendix D. We require equations describing the motions of the particles, and Maxwell's equations to describe the electric and magnetic fields.

The equations of motion are derived from the second moments of the Boltzmann equations (see e.g., Spitzer,[11] p. 94) for ions and electrons:

$$n_e m_e \left[\frac{\partial \underset{\sim}{v}_e}{\partial t} + \underset{\sim}{v}_e \cdot \nabla \underset{\sim}{v}_e\right] = - n_e e \underset{\sim}{E} - n_e e \underset{\sim}{v}_e \times \underset{\sim}{B} - \nabla p_e + \underset{\sim}{P}^{ei} + \underset{\sim}{P}^{en}; \qquad (2.1)$$

$$n_i m_i \left[\frac{\partial \underset{\sim}{v}_i}{\partial t} + \underset{\sim}{v}_i \cdot \nabla \underset{\sim}{v}_i\right] = n_i e \underset{\sim}{E} + n_i e \underset{\sim}{v}_i \times \underset{\sim}{B} - \nabla p_i + \underset{\sim}{P}^{ie} + \underset{\sim}{P}^{in}, \qquad (2.2)$$

where $\underset{\sim}{v}_i$ and $\underset{\sim}{v}_e$ are the ion and electron mass average velocities, respectively, n_i and n_e are the corresponding particle densities, $\underset{\sim}{E}$ is electric field strength, $\underset{\sim}{B}$ is magnetic field strength, p is pressure (viscous effects are neglected–for a justification see p. 66), and $\underset{\sim}{P}^{ij}$ is the momentum transferred per unit time per unit volume from the jth to the ith particle species ($\underset{\sim}{P}^{ij} = -\underset{\sim}{P}^{ji}$). The superscript n in these equations refers to neutral particles.

We now make a number of approximations. We assume that in the equilibrium state $\underset{\sim}{v}$ and $\underset{\sim}{E}$ are zero and $\underset{\sim}{B}$ equals $\underset{\sim}{B}_0$, the static axial magnetic field. Departures from equilibrium are assumed small, so that $\underset{\sim}{B}$ is replaced in these equations by $\underset{\sim}{B}_0$ and the $\underset{\sim}{v} \cdot \nabla \underset{\sim}{v}$ terms are dropped. We also assume that ∇p is negligible.[12] Charge neutrality is assumed (see, e.g., Ref. 33, p. 62), so $n_i = n_e = n$ and the $\underset{\sim}{P}^{ij}$ are taken to be proportional to the relative average velocities $(\underset{\sim}{v}_j - \underset{\sim}{v}_i)$ of the two species involved. This has been shown by Rosenbluth

and Kaufman[13] to be valid for momentum transfer between ions and electrons in plasmas where collisions are infrequent and $\nabla kT = 0$. The assumption seems to be reasonable in the case (of interest in this experiment) of high collision frequency, but has not been proved for this case. The proportionality factors are defined by

$$\gamma = \frac{P^{ni}}{v_i - v_n} \tag{2.3}$$

and

$$\underset{\sim}{\eta} \cdot \underset{\sim}{j} = \frac{\underset{\sim}{P}^{ei}}{en}, \tag{2.4}$$

where

$$\underset{\sim}{j} = en (\underset{\sim}{v}_i - \underset{\sim}{v}_e). \tag{2.5}$$

The factor $\underset{\sim}{\eta}$ is the resistivity of the plasma, and is a tensor.

To obtain an equation of motion, we add Eqs. (2.1) and (2.2), giving

$$n \frac{\partial}{\partial t} (m_e \underset{\sim}{v}_e + m_i \underset{\sim}{v}_i) = \underset{\sim}{j} \times \underset{\sim}{B}_0 + \underset{\sim}{P}^{en} + \underset{\sim}{P}^{in}. \tag{2.6}$$

The ion-electron momentum transfer terms have canceled out. Substituting $\underset{\sim}{v}_e$ from (2.5) into (2.6) gives

$$nm_e \frac{\partial \underset{\sim}{v}_i}{\partial t} - \frac{m_e}{e} \frac{\partial \underset{\sim}{j}}{\partial t} + nm_i \frac{\partial \underset{\sim}{v}_i}{\partial t} = \underset{\sim}{j} \times \underset{\sim}{B}_0 + \underset{\sim}{P}^{in} + \underset{\sim}{P}^{en}. \tag{2.7}$$

The first term on the left is of order m_e/m_i compared with the third term, and for waves of angular frequency ω, the second term is of order ω/ω_{ce} compared with the first term on the right, where ω_{ce} is the electron cyclotron frequency, (refer to Eq. (A1), Appendix A). ω_{ce} is very much larger than the wave frequencies of interest here, so to a good approximation we neglect the first two terms. Also P^{en} may be shown to be of order $\sqrt{\frac{me}{m_i}}$ compared with P^{in}, and is accordingly

dropped. When we use Eq. (2.3) this equation becomes

$$\rho_i \frac{\partial \underset{\sim}{v}_i}{\partial t} = \underset{\sim}{j} \times \underset{\sim}{B}_0 - \gamma(\underset{\sim}{v}_i - \underset{\sim}{v}_n), \tag{2.8}$$

where $\rho_i \equiv nm_i$.

We obtain Ohm's law by substituting $\underset{\sim}{v}_e$ from Eq. (2.5) into Eq. (2.1) and using Eq. (2.4). Again dropping terms of order ω/ω_{ce}, we obtain

$$\underset{\sim}{E} + \underset{\sim}{v}_i \times \underset{\sim}{B}_0 = \underset{\sim}{\eta} \cdot \underset{\sim}{j} + \frac{1}{en} \underset{\sim}{j} \times \underset{\sim}{B}_0 . \tag{2.9}$$

The set of equations is completed by writing Maxwell's equations in linearized form:

$$\nabla \times \underset{\sim}{b} = \mu_0 \underset{\sim}{j} \tag{2.10}$$

$$\nabla \times \underset{\sim}{E} = - \frac{\partial \underset{\sim}{b}}{\partial t} . \tag{2.11}$$

The displacement current term of Eq. (2.10) has been dropped, since it is of the order of the square of the ratio, assumed small, of Alfvén speed to the speed of light. The four equations, (2.8), (2.9), (2.10), and (2.11), constitute the set to be solved.

B. Derivation of Dispersion Relations

We look for departures from equilibrium that are cylindrically symmetric and harmonic in time, so wave quantities vary as $e^{-i\omega t}$, and $\partial/\partial t$ is replaced by $-i\omega$. The term $\gamma(\underset{\sim}{v}_i - \underset{\sim}{v}_n)$ in Eq. (2.8) is shown in Appendix A to be equal to $-i\omega\rho_n[1/(1-i\tau)]$, where $\tau \equiv (\omega/\nu_{ni})$, ν_{ni} is the neutral-ion collision frequency per neutral, and ρ_n is the neutral-particle mass density. With these substitutions, Eq. (2.8) becomes

$$-i\omega\rho_1 \underset{\sim}{v}_i = \underset{\sim}{j} \times \underset{\sim}{B}_0 \,, \tag{2.12}$$

where

$$\rho_1 \equiv \rho_0(1+i\xi) \,; \quad \rho_0 \equiv \rho_i + \rho_n \frac{1}{1+\tau^2} \,; \quad \xi \equiv \frac{\rho_n}{\rho_0} \frac{\tau}{1+\tau^2}$$

We now obtain from Eqs. (2.9), (2.10), (2.11) and (2.12) the wave magnetic field $\underset{\sim}{b}$ (for details see Appendix B). The result is

$$\underset{\sim}{b} = -\frac{V^2}{\omega^2} \nabla \times \left\{ [(\nabla \times \underset{\sim}{b}) \times \hat{z}] \times \hat{z} \right\} - i \frac{1}{\omega \mu_0} \nabla \times (\eta \cdot \nabla \times \underset{\sim}{b})$$

$$- i \frac{\rho_1}{n m_i} \frac{V^2}{\omega \omega_{ci}} \nabla \times \left\{ (\nabla \times \underset{\sim}{b}) \times \hat{z} \right\} , \tag{2.13}$$

where we have introduced the notations

$$V^2 \equiv \frac{B_0^2}{\mu_0 \rho_1} ,$$

$$\omega_{ci} \equiv \frac{eB_0}{m_i} ,$$

and

$$\hat{z} = \underset{\sim}{B}_0 / B_0 .$$

Some vector manipulations with this equation will lead (see Appendix B for details) to

$$\frac{\omega^2}{V^2} \underset{\sim}{b} + \frac{\partial^2}{\partial z^2} \underset{\sim}{b} + \nabla^2 b_z \hat{z} - \nabla \frac{\partial b_z}{\partial z} + i \frac{\omega}{\mu_0 V^2} \nabla \times (\eta \cdot \nabla \times \underset{\sim}{b})$$

$$+ i\Omega \nabla \times \frac{\partial}{\partial z} \underset{\sim}{b} = 0, \tag{2.14}$$

where $\Omega \equiv \frac{\rho_1}{nm_i} \frac{\omega}{\omega_{ci}}$.

We now obtain three separate scalar equations by separating out the $\hat{r}$, $\hat{\theta}$, and $\hat{z}$ components of this equation in cylindrical coordinates. We look for solutions of the form $f(r) \exp[-i(\omega t - pz)]$. It is convenient here to assume $\underline{\underline{\eta}} = \eta_{\parallel} \hat{z}\hat{z} + \eta_{\perp}(\underline{\underline{I}} - \hat{z}\hat{z})$, where $\underline{\underline{I}}$ is the unit tensor, and to introduce the dimensionless numbers

$$a_{\perp} \equiv \frac{\omega \eta_{\perp}}{\mu_0 V^2} \quad \text{and} \quad a_{\parallel} \equiv \frac{\omega \eta_{\parallel}}{\mu_0 V^2}.$$

The three component equations are:

$\underline{r}$

$$-ia_{\perp}\left[\frac{1}{r}\frac{\partial}{\partial r} r \frac{\partial b_r}{\partial r}\right] + \left[-p^2 + \frac{ia_{\perp}}{r^2} + ia_{\perp}p^2 + \frac{\omega^2}{V^2}\right] b_r + ip^2 \Omega b_{\theta} - ip \frac{\partial b_z}{\partial r} = 0; \tag{2.15}$$

$\underline{\theta}$

$$-a_{\parallel}\left[\frac{1}{r}\frac{\partial}{\partial r} r \frac{\partial b_{\theta}}{\partial r}\right] + \left[-p^2 + \frac{ia_{\parallel}}{r^2} + ia_{\perp}p^2 + \frac{\omega^2}{V^2}\right] b_{\theta} - ip^2 \Omega b_r + p\Omega \frac{\partial b_z}{\partial r} = 0; \tag{2.16}$$

$\underline{z}$

$$(1 - ia_{\perp})\left[\frac{1}{r}\frac{\partial}{\partial r} r \frac{\partial b_z}{\partial r}\right] + \left[\frac{\omega^2}{V^2} - p^2(1 - ia_{\perp})\right] b_z - p\Omega\left[\frac{\partial b_{\theta}}{\partial r} + \frac{1}{r} b_{\theta}\right] = 0. \tag{2.17}$$

Note now that if we differentiate the last equation with respect to r, and define an operator

$$S = \frac{1}{r}\frac{\partial}{dr}\left[r \frac{\partial}{dr}\right] - \frac{1}{r^2},$$

then we can write these equations as

$$
\begin{aligned}
&(-ia_{\perp} S + F)\, b_r + ip^2 \Omega b_\theta - ip \frac{\partial b_z}{\partial r} = 0; \\
&(-ia_{\parallel} S + F)\, b_\theta - ip^2 \Omega b_r + p\Omega \frac{\partial b_z}{\partial r} = 0; \qquad (2.18) \\
&\left[(1 - ia_{\perp})S + F\right] \frac{\partial b_z}{\partial r} - p\Omega S b_\theta = 0;
\end{aligned}
$$

where $F \equiv \omega^2/V^2 - (1-ia_{\perp})\, p^2$. By use of $\nabla \cdot \underset{\sim}{b} = 0$ we can eliminate $\partial b_z/\partial r$ from these equations, and we find that the last equation contains the same information as the first. Some manipulation with this set will then show that it may be written as a fourth degree scalar operator operating on a new vector

$$
(S + {}_1k_c^2)\,(S + {}_2k_c^2)\left[b_r \hat{r} + b_\theta \hat{\theta} - \partial b_z/\partial r\, \hat{z}\right] = 0 , \qquad (2.19)
$$

where the ${}_ik_c$ are defined by

$$
{}_{1}^{2}\, k_c^2 = 1/2\left[u \pm (u^2 - 4w)^{1/2}\right], \qquad (2.20)
$$

and

$$
u \equiv \frac{-p^2\Omega^2 - F(1-ia_{\perp} - ia_{\parallel})}{ia_{\parallel}(1-ia_{\perp})} \qquad (2.21)
$$

and

$$
w \equiv \frac{p^4\Omega^2 - F^2}{ia_{\parallel}(1 - ia_{\perp})} . \qquad (2.22)
$$

The solutions to Eq. (2.19) are now easily found for each of the components, since $S + {}_ik_c^2$ is just Bessel's operator for the first order Bessel function. The result for b_r is

$$b_r = \sum_{i=1,2} \left[A_{1i} J_1({}_i k_c r) + A_{2i} N_1({}_i k_c r) \right] \qquad (2.23)$$

with the same solutions, except for the coefficients, for b_θ and $\partial b_z/\partial r$. The requirement that axial current density at $r = 0$ be finite imposes the condition that the coefficients of the Neumann functions be all zero. In deriving Eq. (2.19) we have divided through by $a_\parallel$. If $a = 0$, this step is not permitted; instead we find that the term in S^2 disappears, and the solution for b_r then involves only a single k_c.

In general the boundary conditions on a given problem will require the use of both of the ${}_i k_c$. In cases of this sort it does not seem to be profitable to attempt to break the wave propagation into modes. However, in the rather special case that has been found to hold in the experiment described in this paper (see Section F), it is sufficient to use only a single term. Then the dispersion relation is given by Eq. (2.20), which may be rewritten

$$\Omega^2 p^2 (k_c^2 + p^2) - D_\parallel (D_\perp - k_c^2) = 0 , \qquad (2.24)$$

where we have defined $D_\parallel \equiv (\omega^2/V^2) - (1 - i a_\perp) p^2 + i a_\parallel k_c^2$ and $D_\perp \equiv (\omega^2/V^2) - (1 - i a_\perp) p^2 + i a_\perp k_c^2$.

Equation (2.24) yields two solutions for p^2, each of which may be described as a wave mode, and which have a direct connection with the wave modes described by other authors. The solutions are

$$p_{1,2}^2 = \frac{-b \pm [b^2 - 4ac]^{1/2}}{2a}, \tag{2.25}$$

where

$$a = \Omega^2 - (1 - i\alpha_\perp)^2,$$

$$b = k_c^2(\Omega^2 - 1) + (\alpha_\perp^2 + \alpha_\perp\alpha_\parallel)k_c^2 + 2(1 - i\alpha_\perp)\frac{\omega^2}{V^2} + (2\alpha_\perp + \alpha_\parallel)\, ik_c^2, \tag{2.26}$$

and

$$c = -\frac{\omega^4}{V^4} + \frac{\omega^2}{V^2} k_c^2 + \alpha_\perp\alpha_\parallel k_c^4 + i\alpha_\parallel\left[k_c^4 - \left(1 + \frac{\alpha_\perp}{\alpha_\parallel}\right)\frac{\omega^2}{V^2} k_c^2\right].$$

C. Wave Types

We identify the different wave types with modes found by other authors by examining them in the limiting case $\Omega = 0$, which corresponds to dropping the $\underset{\sim}{j} \times \underset{\sim}{B}_0$ term of Eq. (2.9). Equation (2.24) for this case becomes $D_\parallel(D_\perp - k_c^2) = 0$. The root labeled p_2 is given by $D_\parallel = 0$, so that the dispersion relation is

$$p_2^2 = \frac{1}{1 - i\alpha_\perp}\left[\frac{\omega^2}{V^2} + i\alpha_\parallel k_c^2\right]. \tag{2.27}$$

This is the wave type labeled the Principal Mode by Newcomb,[14] and in the limit $\alpha = 0$ is also the T-type wave of Gajewski.[15] We shall continue to use Gajewski's nomenclature for these waves. The other root is characterized by the dispersion relation $D_\perp = k_c^2$, which gives

$$p_1^2 = \frac{1}{1 - i\alpha_\perp}\frac{\omega^2}{V^2} - k_c^2. \tag{2.28}$$

This is the wave type called the TE mode by Newcomb, and in the limit where α is zero it is the TLA-type wave of Gajewski.

Using the dispersion relations Eqs. (2.27 and (2.28) with Eqs. (2.18), we find the wave magnetic fields for the two cases. The results are summarized in Table I.

Table I

Wave fields in the limit where the $j \times B_0$ term of Eq. (2.9) can be neglected.

Wave type	T	TLA
Dispersion relation	$p_2^2 = \frac{1}{1 - i\alpha_\perp}\left(\frac{\omega^2}{V^2} + i\alpha_{\|} k_c^2\right)$	$p_1^2 = \frac{1}{1 - i\alpha_\perp}\frac{\omega^2}{V^2} - k_c^2$
b_r	0	$J_1(k_c r)$
b_θ	$J_1(k_c r)$	0
b_z	0	$i\frac{k_c}{p} J_0(k_c r)$

D. Attenuation Constants

For either of the wave types considered, the attenuation caused by finite electrical conductivity is found by breaking the complex propagation constant p^2 into its real and imaginary parts. Since p enters the equations as e^{ipz}, it is seen that the real part of p is the propagation constant k and that the imaginary part represents a damping constant ϵ,

$$p = k + i\epsilon. \tag{2.29}$$

Solving in general for k and ϵ leads to

$$k^2 = \frac{1}{2}\,\mathrm{Re}(p^2)\left\{1 + \left[1 + \left(\frac{\mathrm{Im}(p^2)}{\mathrm{Re}(p^2)}\right)^2\right]^{1/2}\right\} \tag{2.30}$$

and

$$\epsilon^2 = \frac{1}{2}\,\mathrm{Re}(p^2)\left\{-1 + \left[1 + \left(\frac{\mathrm{Im}(p^2)}{\mathrm{Re}(p^2)}\right)^2\right]^{1/2}\right\} . \tag{2.31}$$

For $[\mathrm{Im}(p^2)/\mathrm{Re}(p^2)]^2 \ll 1$, then approximately,

$$\epsilon = \frac{1}{2}\,\frac{\mathrm{Im}(p^2)}{[\mathrm{Re}(p^2)]^{1/2}} . \tag{2.32}$$

This may also be written simply in terms of k as

$$\epsilon = \frac{\mathrm{Im}(p^2)}{2k} . \tag{2.33}$$

E. Limiting Cases

The relation Eq. (2.25) written out in its entirety is

$$p_{\frac{1}{2}}^2 = \frac{k_c^2}{2(1-i\alpha)^2 - 2\Omega^2}\left\{-(1-\Omega^2) + 2\beta^2(1-i\alpha) + 2\alpha^2 + 3i\alpha \mp \left[(1-\Omega^2)^2 + 4\Omega^2\beta^4 - \alpha^2 + i\alpha\left(2(\Omega^2-1) + 4\Omega^2\beta^2\right)\right]^{1/2}\right\} , \tag{2.34}$$

where we have introduced the dimensionless number $\beta^2 \equiv \omega^2/V^2k_c^2$. It is possible to carry the tensor resistivity further in the discussion, but we here take $\alpha_\perp = \alpha_{||} = \alpha$ for simplicity. We shall look briefly at the limiting cases of Eq. (2.34) for low frequency compared with ion cyclotron frequency ($\omega \ll \omega_{ci}$), frequencies near ion cyclotron frequency

($\omega \approx \omega_{ci}$), and small but finite resistivity ($\alpha \ll 1$). Because of the presence of neutral atoms, V^2 is complex (due to ρ_1); therefore both α and β are complex. Also, Ω has an imaginary part due to neutrals. In the following discussion we assume the imaginary parts of α, β, Ω to be very much smaller than their respective real parts.

1. Low Frequency ($\omega \ll \omega_{ci}$)

In this case, as long as $\beta^4 \Omega^2 \ll 1$ and $\alpha \ll 1$, the T-wave dispersion relation becomes

$$p_2^2 = \frac{k_c^2}{1 - i\alpha}(\beta^2 + i\alpha)\left[1 + \frac{\Omega^2(1+\beta^2)}{(1 - i\alpha)^2}\right]. \qquad (2.35)$$

This is the relation appropriate to the experimental work described in this paper. The TLA-wave dispersion relation under the same assumptions is

$$p_1^2 = \frac{1}{1 - i\alpha}\frac{\omega^2}{V^2} = k_c^2 - \Omega^2\frac{\omega^2}{V^2}\,\frac{1 - \beta^2 + i\alpha}{(1 - i\alpha)^3}. \qquad (2.36)$$

2. Frequencies Near Ion Cyclotron Frequency

We first look at the limit of zero resistivity, i.e., $\alpha = 0$. In this case Eq. (2.34) simplifies to

$$p_{1,2}^2 = \frac{k_c^2}{2}\left\{\frac{2\beta^2}{1-\Omega^2} \pm \left[1 \pm (1 + 4\beta^4\frac{\Omega^2}{(1-\Omega^2)^2})^{1/2}\right]\right\} \qquad (2.37)$$

For $\Omega \to 1$, the second term in the square root becomes large compared with the first. Expanding the square root bracket in powers of the reciprocal of the second term leads to

$$\left[1 + 4\beta^4\frac{\Omega^2}{(1-\Omega^2)^2}\right]^{1/2} \approx 2\beta^2\frac{\Omega}{1-\Omega^2} + \frac{1-\Omega^2}{4\beta^2\Omega}. \qquad (2.38)$$

Putting this into (2.37), we find, for the limiting cases,

$$\left.\begin{aligned} p_1^2 &= \frac{\omega^2}{V^2}\left[\frac{1}{1+\Omega} - \frac{1}{2\beta^2} - \frac{1-\Omega^2}{8\beta^4\Omega}\right] \qquad \text{(TLA)} \\ \text{and} \\ p_2^2 &= \frac{\omega^2}{V^2}\left[\frac{1}{1-\Omega} - \frac{1}{2\beta^2} + \frac{1-\Omega^2}{8\beta^4\Omega}\right] \qquad \text{(T)} \end{aligned}\right\} \quad (2.39)$$

Owing to the term $(1-\Omega)^{-1}$ in the T equation, p_2 goes to infinity at the ion cyclotron frequency, and the group velocity of this wave goes to zero. Thus this mode has a resonance at the ion cyclotron frequency. This is the mode discussed by Stix.[16] The TLA wave has no resonance, since the $(1-\Omega)^{-1}$ term does not appear.

The waves represented by Eq. (2.37) are propagating types only if p^2 is positive. For the T wave, p_2^2 is always positive for $\Omega < 1$. However, for the TLA wave the condition that p_1^2 be positive is

$$\frac{2\beta^2}{1-\Omega^2} \geq 1 + \left[1 + 4\beta^4 \frac{\Omega^2}{(1-\Omega^2)^2}\right]^{1/2}, \qquad (2.40)$$

which is always satisfied for $\beta \geq 1$. This is the same cutoff condition one would obtain directly from Eq. (2.28).

It is interesting to see the effect of a small but finite resistivity on the resonant (T) mode near resonance. For the conditions $(1-\Omega^2) \ll 2\Omega\beta^2$ and $a^2 \ll 1-\Omega^2$,

$$p_2^2 = \frac{1}{1-\Omega}\left[\frac{\omega^2}{V^2} + iak_c^2\right] + \frac{ia}{(1-\Omega)^2}\frac{\omega^2}{V^2}. \qquad (2.41)$$

The attenuation constant ϵ is the imaginary part of p and is calculated using Eq. (2.31) to be

$$\epsilon \approx \frac{\omega}{2V} \quad \frac{a}{(1-\Omega)^{3/2}} \quad . \tag{2.42}$$

Thus, near ion cyclotron frequency, one would expect ohmic damping to become relatively large.

F. Wave Fields

The $_{i}k_{c}$ are determined by a boundary condition at the tube wall ($r = b$). The effective boundary condition has been found experimentally to be $j_r(b) = b_\theta(b) = 0$, probably due to the presence of a poorly conducting layer of gas at the tube wall (see section on Radial Distributions of b_θ Fields). If the thickness of this layer lies within certain limits, it can be shown (see Appendix F) that it is only necessary to consider a single term of Eq. (2.23) (thus we may drop the subscript i), and that k_c is determined by

$$J_1(k_c b) = 0 \ , \tag{2.42a}$$

where b is the radius of the tube wall. Since this condition may be met by an infinite number of discrete k_c, the general solution must be expressed as an infinite series of Bessel functions. Eq. (2.23) for b_r now becomes

$$b_r = \sum_{n=1}^{\infty} A_n J_1(k_{cn} r) \ . \tag{2.43}$$

Utilizing div $\underset{\sim}{b} = 0$, we obtain

$$b_z = - \sum_{n=1}^{\infty} \frac{k_{cn}}{ip_n} A_n J_0(k_{cn} r) \ . \tag{2.44}$$

We write the equation for b_θ as

$$b_\theta = \sum_{n=1}^{\infty} C_n J_1(k_{cn} r) , \tag{2.45}$$

noting that C_n and A_n are related by any of Eqs. (2.18). The first of these gives

$$-ip^2 \Omega C_n = (D_\perp - k_{cn}^2) A_n . \tag{2.45a}$$

The other wave fields can be obtained through substitution of this set into Eqs. (2.9) through (2.12). The results are, for the nth mode,

$$j_r = -i \frac{p_n}{\mu_0} C_n J_1(k_{cn} r) , \tag{2.46}$$

$$j_\theta = \frac{i}{\mu_0 p_n} \left(p_n^2 + k_{cn}^2 \right) A_n J_1(k_{cn} r), \tag{2.47}$$

$$j_z = \frac{k_{cn}}{\mu_0} C_n J_0(k_{cn} r) , \tag{2.48}$$

$$v_{ir} = - \frac{V^2}{\omega B_0 p_n} \left(p_n^2 + k_{cn}^2 \right) A_n J_1(k_{cn} r), \tag{2.49}$$

$$v_{i\theta} = -\frac{p_n V^2}{\omega B_0} C_n J_1(k_{cn} r) , \tag{2.50}$$

$$v_{iz} = 0 , \tag{2.51}$$

$$E_r = \frac{V^2}{\omega p_n} \left[(1 - i\alpha) p_n^2 C_n + i\Omega \left(p_n^2 + k_{cn}^2 \right) A_n \right] J_1(k_{cn} r) , \tag{2.52}$$

$$E_\theta = - \frac{\omega}{p} A_n J_1(k_{cn} r) , \tag{2.53}$$

and

$$E_z = \frac{k_{cn} V^2}{\omega} \alpha C_n J_0(k_{cn} r) , \tag{2.54}$$

where we have omitted the factor $\exp[-i(\omega t - p_n z)]$ everywhere. For $\Omega = 0$, we find again the results of Table I, where the T-type wave is given by setting $A_n = 0$, and the TLA wave by setting $C_n = 0$. In the general case, for $\Omega \neq 0$, each mode involves both the A_n and the C_n. For small Ω and a, the T-type wave has $A_n = -i\Omega\beta_n^2 C_n$, while for the TLA type $C_n = -i\Omega\beta_n^2 A_n$. In the experimental work of this paper we examine the T wave, for which Ω is approx 0.025 and β_0^2 is approx 0.025, so to good approximation we can consider the A_n to be zero. Also note that to this order of approximation $\operatorname{div} \underset{\sim}{v}_i = 0$, which justifies the neglect of pressure effects for these waves.

The wave fields for both types of waves are shown in the diagram of Fig. 2. Note that in both types the currents are confined to the plasma, and do not enter the wall.

G. T Waves

The T-type wave is the subject of the experimental work undertaken here, so we examine it in more detail. To avoid confusion, the subscript n designating radial mode number is dropped in the following discussion through Eq. (2.58). In order to orient the discussion, we present a few typical values of pertinent parameters:

$a < 0.015$,
$\Omega \leq 0.025$,
$k_{c1} = 55.5\ m^{-1}$,
$\beta \leq 0.2$
$\nu_{ni} \sim 5\times10^7\ sec^{-1}$
$\omega \sim 4\times10^6\ sec^{-1}$,
$\xi \sim 0.01$.

Under these conditions, the dispersion relation Eq. (2.35) is valid. If we calculate the dependence of k on ω from this equation we obtain, for $\omega << \omega_1$ (where we define $\omega_1 \equiv \eta k_c^2/2\mu_0$),

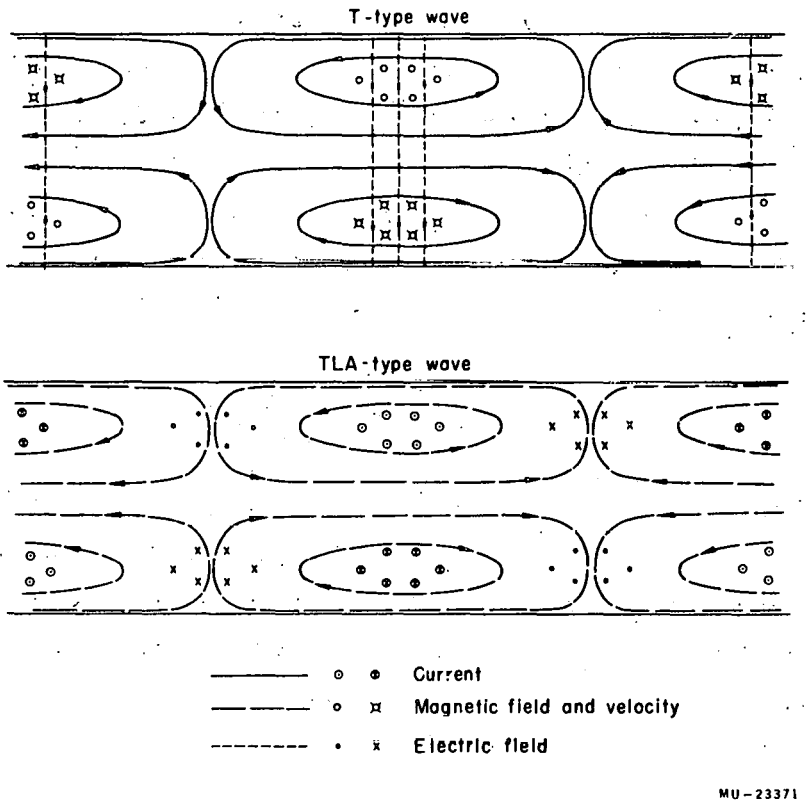

Fig. 2. Schematic diagram of wave fields in hydromagnetic waveguide for low frequencies and zero damping. The static axial magnetic field is not shown.

$$k^2 = \frac{\omega\omega_1}{V^2}, \tag{2.55}$$

while for $\omega_1 << \omega << \omega_{ci}$

$$k^2 = \frac{\omega^2}{V^2}. \tag{2.56}$$

For experimental work ω_1 is approximately 5×10^5 sec^{-1}. When Eq. (2.56) is valid, $\beta = k/k_c$ and $\alpha = \delta^2 k^2/2$, where $\delta = \sqrt{2\eta/\omega\mu_0}$ is the customary skin depth for penetration of electromagnetic fields into a conductor. The turnover point for k at $\omega = \omega_1$ occurs when the skin depth has become just equal to a radial wavelength defined by 2 times the reciprocal of the radial wave number k_c. From Eq. (2.39) we see that as ω approaches ω_{ci} k tends toward infinity. Inclusion of resistivity causes k to turn over very near to ω_{ci} and go to zero.

Attenuation of the wave is primarily due to two effects-ohmic losses in the plasma arising from electron-ion collisions, and collisions of ions with neutrals that end to destroy the ordered ion motion. The imaginary part of p in Eq. (2.35) is an attenuation constant, and is calculated for $\omega << \omega_1$ to be

$$\epsilon \approx \left[\frac{\omega_1\omega}{V^2}\right]^{1/2} \tag{2.57}$$

In this frequency range then, $\epsilon = k$, so waves are attenuated to 1/e in a distance equal to $1/2\pi$ times a wavelength. For $\omega_1 << \omega << \omega_{ci}$ and $\frac{\omega}{\nu_{ni}} << 1$:

$$\epsilon = \epsilon_j + \epsilon_n = \frac{\eta}{2\mu_0 V}\left(\frac{\omega^2}{V^2} + k_c^2\right) + \frac{1}{V}\frac{\omega^2}{\nu_{ni}}\frac{\rho_n}{\rho_0}. \tag{2.58}$$

The first term in Eq. (2.56) expresses the damping due to joule losses ϵ_j; the second term is the damping due to the presence of neutrals ϵ_n. The expression for ϵ_j may be calculated directly from Eq. (2.27), from which it can be seen that the η that appears in Eq. (2.58) is the parallel resistivity $\eta_{||}$. In Fig. 3 the propagation and attenuation factors are presented graphically as functions of ω. In much of the experimental work, the induced waveform is a single pulse resembling a half-sine wave of 0.8 μsec duration. The approximate frequency spectrum of this pulse is also shown in Fig. 3. When a ringing waveform was used, the frequency was $\omega = 3\times10^6$ sec^{-1}. Over a fairly wide band of frequencies, including the dominant experimental frequencies, k is equal to ω/V and ϵ_j is almost independent of frequency, while ϵ_n is negligible. The variations in k from ω/V occur at frequencies low enough that the effect on the observed velocity of the pulse is small.

H. Analysis of Initial Disturbance into Radial Modes

The coefficients C_n of the T-type wave which appear in Eqs. (2.43) through (2.54) are the amplitudes of the various radial modes. The relative amplitudes of these modes are determined by the manner in which the wave is excited, i.e., by the geometry of the driving electrodes. The fields produced by the source of excitation can be analyzed into the radial normal modes of the waveguide, which form a complete orthogonal set.[17, 18] Such an analysis is somewhat difficult for the case of finite conductivity, but for the case of zero damping a simple analysis can be made. We make the analysis for the latter case to find the relative amplitudes of the various modes at the excitation end, and then somewhat arbitrarily we apply the damping of Eq. (2.58) to these modal amplitudes, in order to find the wave fields at any point in the tube. To make the necessary expansion, we must know the boundary condition at the tube wall (r = b). This is the condition which will determine the k_{cn}.

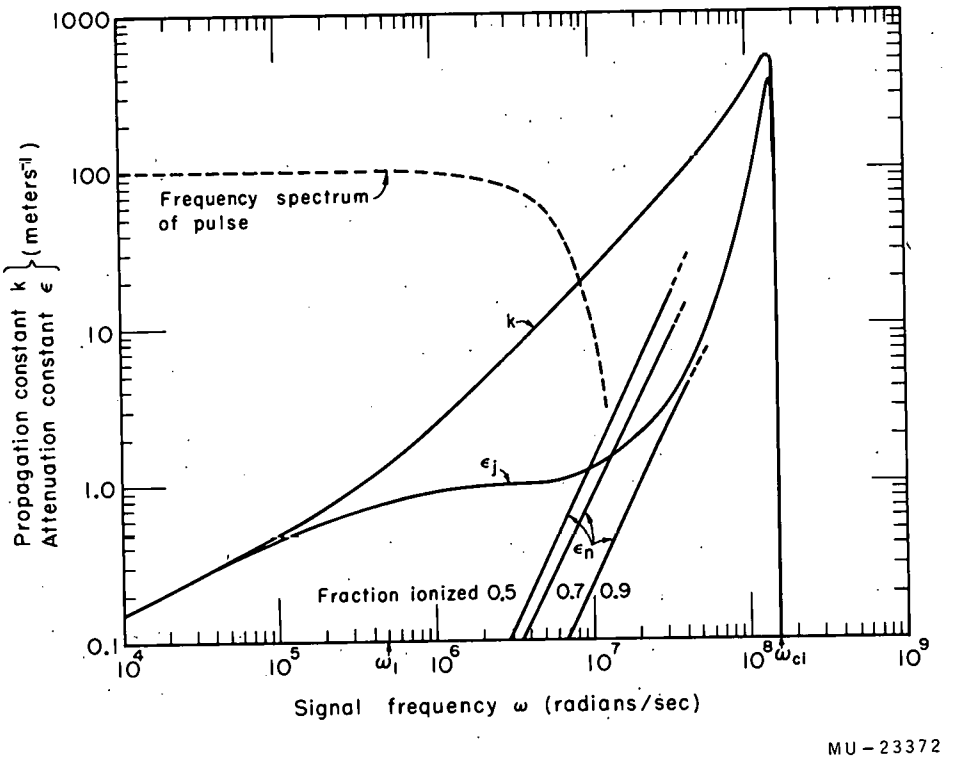

Fig. 3. Propagation and attenuation constants as a function of frequency. Conditions are: B_0=16 kgauss, $\rho=10^{-8}$ gm/cm^3, T=10^4 °K, $\nu_{ni}=10^8$, and for k and ϵ_j curves, 90% ionization. The curve labeled k is the real part of the propagation constant p_2. Note that in the range around $\omega=4\times10^6$ sec^{-1} the relationship between k and ω is linear. ϵ_j is the attenuation constant for resistive damping, and ϵ_n in the attenuation constant for neutral particle damping shown for various particle percentages. ω_1 is defined in the text, and ω_{ci} is the ion cyclotron frequency. The dashed curve is the approximate frequency spectrum of the pulse used in some of the experiments.

It has been found experimentally that the radial wave current density j_r is zero at the tube wall (see Sec. IV-d, Radial Distribution of b_θ Field). Equation (2.46) then shows the boundary condition to be $J_1(k_{cn}b) = 0$. This becomes an enigma, since the method of inducing the wave requires a current to flow to the wall. The explanation seems to be that a high-density current from an external source can penetrate the insulating boundary layer that otherwise exists between the plasma and the wall. Experimental evidence concerning this boundary layer is presented below. For the present analysis we approximate this state of affairs with the electrode structure shown in Fig. 4, taking at the end the limit as c approaches b.

The assumed boundary condition at the insulator surface at $z = 0$ is that the axial current density j_z is zero. The curl $\underset{\sim}{b}$ equation (2.10) then shows that $\frac{1}{r}\frac{\partial}{\partial r}(rb_\theta) + \frac{1}{r}\frac{\partial b_r}{\partial \theta} = 0$. If the input circuit has axial symmetry, then $\frac{\partial b_r}{\partial \theta} = 0$, and the resultant equation shows that $b_\theta(r, 0)$ is proportional to $1/r$. At the electrode surfaces at $z = 0$ the tangential electric field is zero. If we now assume $\Omega \ll 1$ and zero damping, reference to Eq. (2.35) shows the p_n all equal. Then, comparison of the equations for E_r and b_θ (2.52) and (2.43) shows that b_θ is proportional to E_r, and is thus also zero at the electrode surfaces. We have then:

$$b_\theta(r, 0) = \begin{cases} 0; \; a < r; \; c < r < b \\ \frac{\mathfrak{I}}{r} \; a < r < c \end{cases} , \tag{2.59}$$

where $\mathfrak{I}$ is a constant.

This function is now equated to Eq. (2.43) at $z = 0$, giving

$$b_\theta(r, 0) = \sum_{n=1}^{\infty} C_n J_1(k_{cn}r) , \tag{2.60}$$

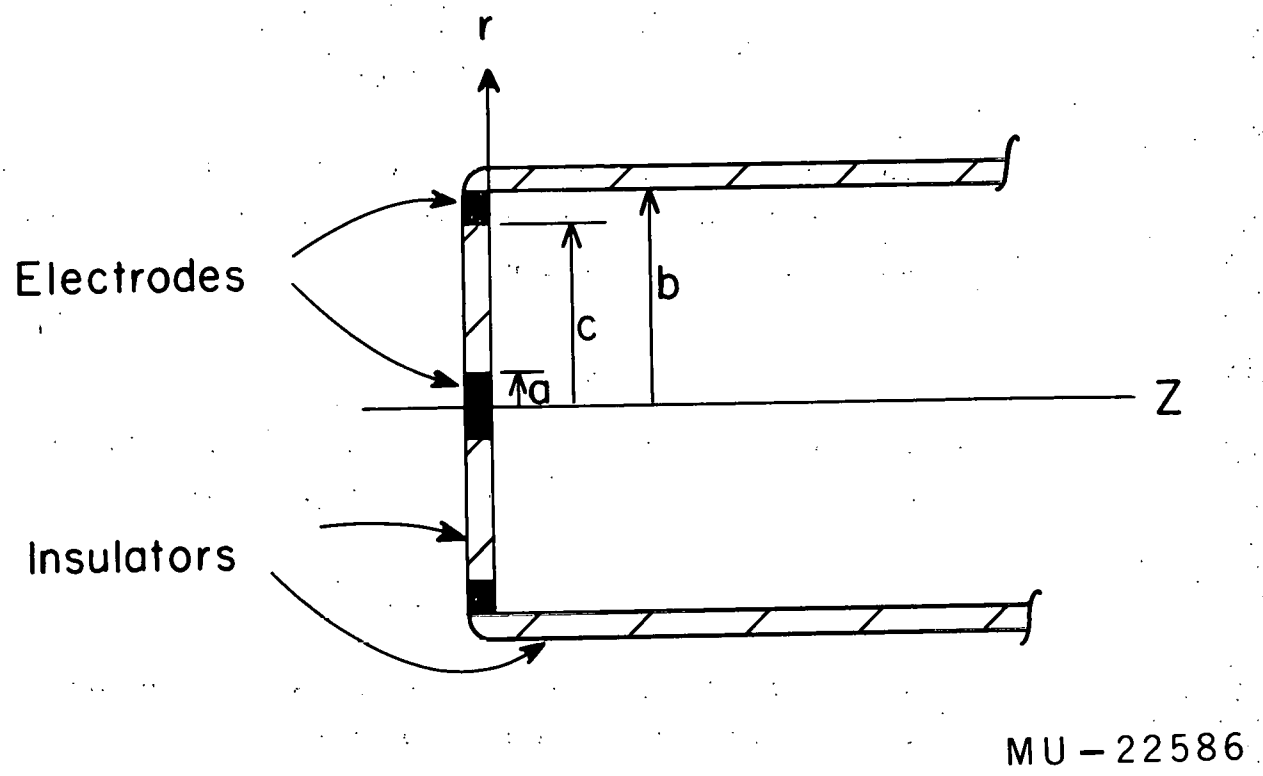

Fig. 4. Electrode arrangement assumed for modal analysis.

where the time dependence has been omitted. To find the C_n, we multiply through on both sides by $J_1(k_{cn}r)\,r\,dr$, integrate over the interval $0 < r < b$, and go to the limit as c approaches b. Because of the orthogonality of the functions only one term survives, and we obtain

$$C_n = \frac{-2\mathfrak{I}}{b^2} \frac{J_0(k_{cn}b) - J_0(k_{cn}a)}{k_{cn}J_0^{\,2}(k_{cn}b)} . \tag{2.61}$$

The constant $\mathfrak{I}$ is determined by matching the vacuum magnetic field $b_{\theta vac}$ in the insulator to the magnetic field $b_\theta(r, 0)$ in the plasma. The vacuum field, again assuming a symmetrical drive, is

$$b_{\theta vac} = \frac{\mu_0 I}{2\pi r} , \tag{2.62}$$

where I is the total current flowing to the electrode. Comparison of the preceeding expression with Eq. (2.59) now shows that

$$\mathfrak{I} = \frac{\mu_0 I}{2\pi} . \tag{2.63}$$

This constant may also be expressed in terms of the applied voltage V_0. It has already been shown that for zero resistivity and low frequency, $E_r(r)$ is proportional to $b_\theta(r)$, hence goes as $1/r$. Integrating $E_r(r)$ between a and b gives the applied voltage V_0, and we find that

$$E_r = \frac{V_0}{r \ln(b/a)} , \tag{2.64}$$

which is the same as the vacuum field. The ratio of E_r to b_θ from Eqs. (2.43) and (2.52) is V, so we obtain

$$b_\theta = \frac{V_0}{r V \ln(b/a)} , \tag{2.65}$$

from which we see

$$\mathcal{S} = \frac{V_0}{V \ln(b/a)} \tag{2.66}$$

Finally, it should be noted that the input impedance is

$$Z_0 = \frac{V_0}{I} = \frac{\mu_0 V}{2\pi} \ln(b/a), \tag{2.67}$$

which is just the characteristic impedance of a coaxial transmission line of inner and outer radii a and b respectively, and filled with a material of dielectric constant

$$K = \frac{\mu_0 \rho C^2}{B_0^2}, \tag{2.68}$$

where C is the speed of light in vacuum. This has previously been shown to be the appropriate dielectric constant for a magnetized plasma (Ref. 11, p. 35).

The ratio of wave energy in any one mode to total wave energy is now easily calculated to be

$$\frac{W_n}{W_T} = \frac{2}{b^2 \ln(b/a)} \left[\frac{J_0(k_{cn}b) - J_0(k_{cn}a)}{k_{cn} J_0(k_{cn}b)} \right]^2 \tag{2.69}$$

In Table II we summarize some of the results of these calculations for conditions of this experiment. The second column shows the energy going into each of the first five modes, expressed as a percentage of total wave energy at the input end. The third column gives the peak value of $b_{\theta n}$ for each of these modes, where $\mathcal{S}$ has been calculated from Eq. (2.66), using for V_0 the observed value of 780 volts. In the fourth column we present the damping lengths (distance in which a wave field attenuates to 1/e of its initial value) calculated from Eq. (2.58). The value of resistivity used was 3.19×10^{-4} ohm-meter and was

experimentally determined by measuring the attenuation of a wave that had traveled far enough so that only the lowest mode was present. Thus the damping length for the n = 1 mode is measured, and the others are calculated using the same value of resistivity. In the last column we have applied the damping of column four to the amplitudes in the third column to obtain the wave amplitudes after one transit through the tube.

Table II

Some results of the modal analysis

Mode number n	Initial energy (% total wave energy)	Initial peak value of b_θ (gauss)	Damping length L (cm)	Peak value of b_θ after one transit (74 cm) (gauss)
1	79	+476	107	238
2	7	-188	32	17.5
3	0.7	- 74	15	0.5
4	4.3	-206	9	0.05
5	2.5	+176	6	--

The lowest mode is excited most strongly (79% of the wave energy goes into this mode), and has considerably less attenuation than the higher modes. After the wave has made one transit through the tube the amplitude of the second mode is already down to 7% of the amplitude of the lowest mode, and higher modes are present to a negligible extent.

III. EXPERIMENTAL METHOD

The cylindrical geometry was chosen as the best possible compromise between situations amenable to theoretical calculation and those in which experimental difficulties are minimized. A copper tube is placed in a uniform axial magnetic field, and is filled with a plasma. A small disturbance is then introduced into the plasma at one end of the tube, and the resulting waves are examined. In particular, it is possible experimentally to look for wave magnetic fields in the body of the plasma with small magnetic field probes; integrated radial electric fields appearing as voltages on coaxial electrodes; and radial currents flowing to the tube walls detected by means of radial current probes in the wall of the tube.

A. Apparatus

The hydromagnetic waveguide is a copper tube (Fig. 1), 14.3 cm diam $\times$ 86.3 cm long. The ends of the tube are closed by pyrex plates through which coaxial molybdenum electrodes may be inserted. A water-cooled solenoid surrounds the tube, and provides a magnetic field variable from zero to about 16 kilogauss. Current to these coils is supplied from a silicon rectifier power supply and from a motor-generator set. The field is uniform to within 1/2% over radius, and to within 3% along the central 76 cm of the tube. At the extreme ends, the field is down by 5%. The field was calibrated to within 2%.

A vacuum with a base pressure of 2×10^{-5} mm of Hg is provided by a liquid nitrogen trapped oil diffusion pump. While an experiment is being run, hydrogen gas flows continuously through the tube at a rate sufficient to change the gas once between shots. The pressure of the gas in the tube is monitored with a Pirani vacuum gauge, calibrated periodically against an oil manometer. Unless stated otherwise, all experiments here were made with hydrogen gas at a pressure of 100 μ of Hg.

The ionization energy is supplied by a lumped-constant pulse line, consisting of ten 7.5-μf capacitors connected with 1-μh inductances. Switching is accomplished with two parallel Westinghouse 5550 ignitrons, and two more such ignitrons are connected to short circuit ("crowbar") the bank when desired. It is possible to program the switching operation to within 1 μsec. A 0.8 ohm resistor in series with the output from the pulse line reduces the dependence of the driving current on plasma conditions. The bank is initially charged to 10 kv, and delivers a nearly constant current of about 8000 amps. Current is conducted through six RG/8U cables to the molybdenum electrode on the "driving end" and returns via the tube wall to ground. A resistive voltage divider allows the voltage on this electrode to be monitored by an oscilloscope.

B. Generation of Waves

With a plasma established in the tube, a torsional hydromagnetic wave is induced by discharging a 0.2-μf capacitor between the central electrode and the copper cylinder. This capacitor may be allowed to ring or may be critically damped, depending upon the application. When it is damped, the current pulse is roughly a half-sine wave of 0.8 μsec duration.

C. Wave Diagnostics

A typical probe tube is shown at the right side of Fig. 1. These are 2-mm-diam pyrex tubes, fused onto the pyrex end plate. The magnetic field probe is a 75-turn coil wound on a 1-mm-diam form and oriented to measure one of the three components of the magnetic field. The probe signals are integrated by a 10-μsec time constant integrating circuit and are displayed on Tektronix type 551 oscilloscopes. The pyrex plate on the right side may also be provided for some applications with an electrode identical to the one at the other end, at which the integrated radial electric field may be observed.

Radial currents flowing to the tube walls are measured by means of current probes in the tube walls, one of which is diagrammed in Fig. 5. The probe consists of a small section of the tube wall which has been electrically isolated from the surrounding wall and then connected to the adjacent wall coaxially through a resistance of 0.85 ohm. Current flow to the probe produces a small voltage drop across the resistor, and this voltage is displayed on an oscilloscope.

D. Plasma Preparation

When the ignitrons connecting the capacitor bank to the tube are first switched on, the whole 10 kv of the pulse line is applied to the tube and a local breakdown occurs in the gas at the driving end. The breakdown delay at low gas pressure is made smaller by providing the electrode with a small "spark plug" which produces some initial ionization. Following the local breakdown, a well-defined ionization wave forms and travels down the tube at a velocity determined by gas pressure, axial magnetic field, and current (typically 5 cm/μsec in this experiment). This front is similar to a switch-on shock wave[19] in that a transverse magnetic field and transverse component of velocity are "switched on" at a point as the front passes. It differs in that it passes into a gas that is initially cold and non-conducting. We shall refer to it as a "switch-on ionization wave", or simply as "ionization wave." The wave front is only a few centimeters thick, and behind the front the plasma is rotating due to the $\underset{\sim}{j} \times \underset{\sim}{B}$ forces. The progress of the ionization wave through the gas may be observed by looking at the current density flowing to the tube wall as a function of position along the tube, utilizing the radial current probes. Five such probes were used to measure the position of the wavefront as a function of time, and the results are shown in Fig. 6. The constancy of the front velocity is probably a result of the constant driving current. Figure 7 is an oscillogram of the current and voltage at the driving end of the tube during the transit of the ionizing front.

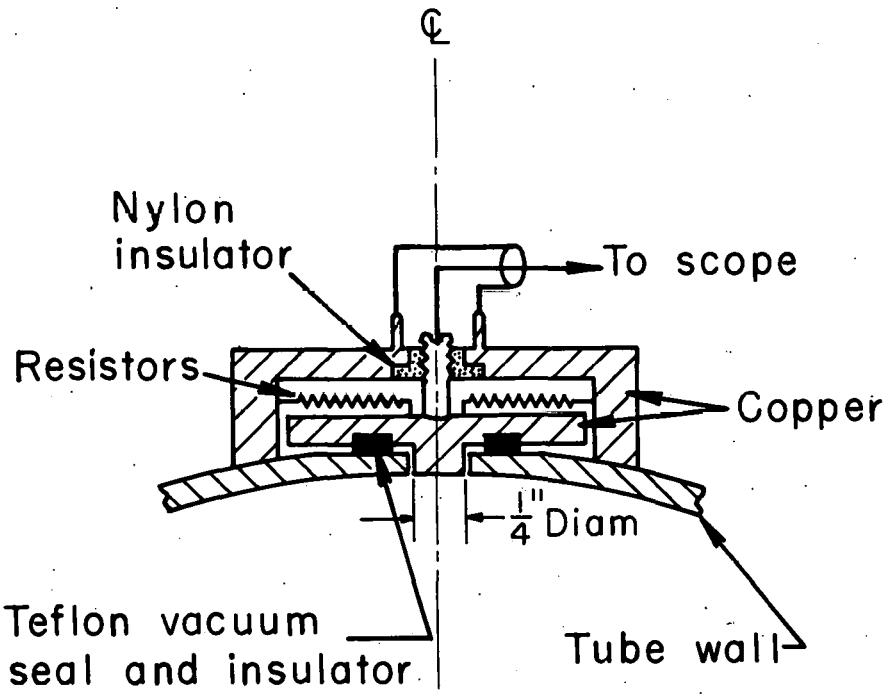

Fig. 5. Geometry of the radial-current probe. The 1/4-inch diameter button is connected to the adjacent wall through six parallel 5-ohm resistors. The maximum voltage drop is less than 1 volt.

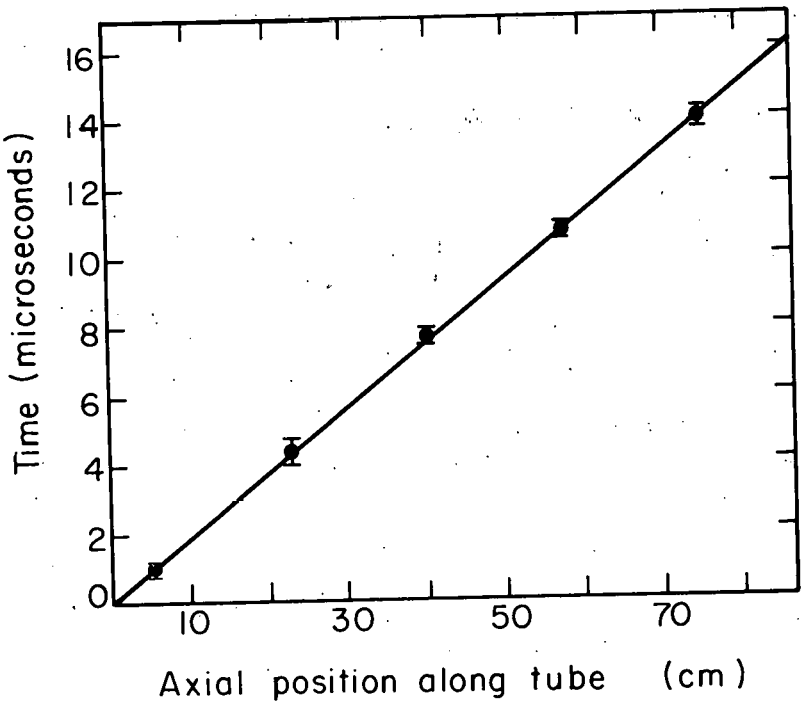

Fig. 6. Position of the ionization front vs time, as measured with radial current probes. The axial magnetic field was 16.0 kgauss, and density was 10^{-8} g/cm^3.

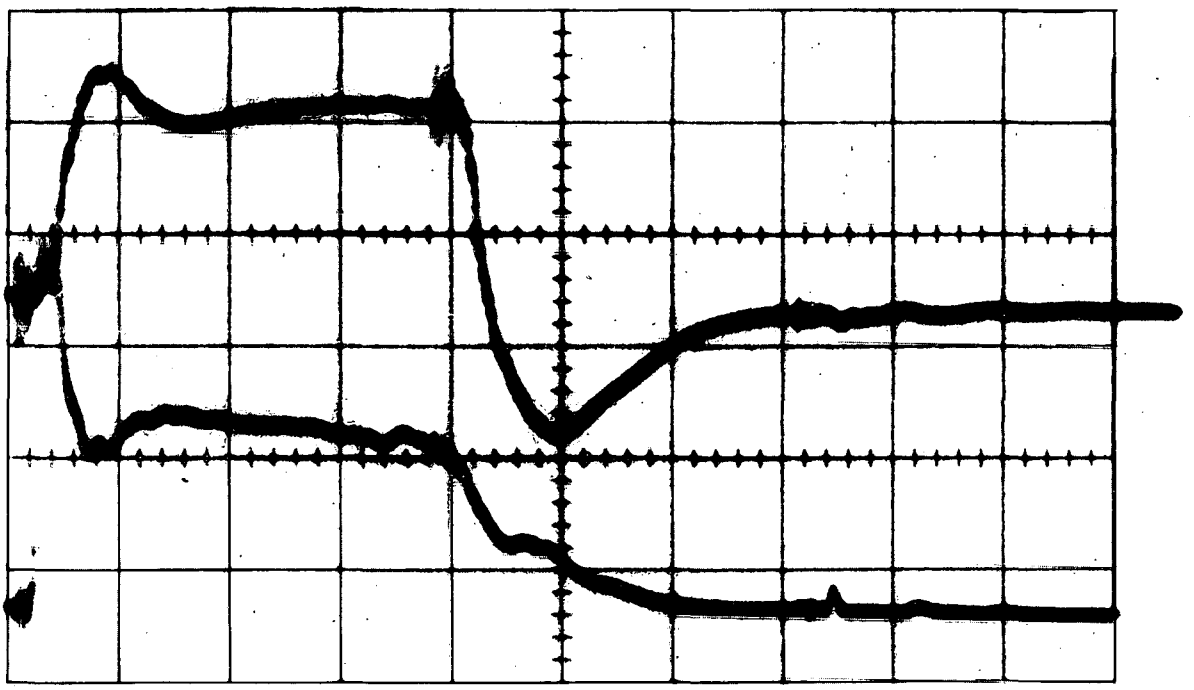

ZN-2756

Fig. 7. Oscilloscope traces showing ionizing conditions. The bottom trace is voltage on the driving coaxial electrode at 2900 volts/cm; the top trace is current from the pulse line at 4700 amp/cm. The horizontal scale is 5 μsec/cm. The current was crowbarred 20 μsec after the voltage was first applied. A single-pulse hydromagnetic wave was induced 37 μsec after the voltage was first applied.

The arrival of the ionization front at the receiving end of the tube may be seen by looking at the voltage drop produced across a small (0.33Ω) resistor connected from a coaxial electrode there to the tube wall. The voltage is zero while the ionization wave is traveling through the plasma, and then rises abruptly at the time the front arrives, as shown in Fig. 8. A similar abrupt rise has been observed in the azimuthal magnetic field upon arrival of the front.

If the receiving end of the tube is not short circuited, and if, after the ionization front has reached the receiving end the driving current is allowed to continue to flow, we observe a drop in the tube resistance, and simultaneously spectral emission lines of materials characteristic of the insulator appear strongly. Therefore, to keep the plasma as clean as possible, the driving current is short-circuited (crowbarred) just as the front reaches the end. Under these conditions the impurity lines appear only weakly. The short-circuit also brakes the spinning plasma to a halt, dissipating the kinetic energy of the plasma in ohmic losses, mainly in the external circuit. Evidence of plasma rotation is seen in the pulse of reverse current that flows from the tube after crowbar.[19a] It is in the decaying plasma so formed that the wave experiments have been performed.

E. Plasma Properties

1. Ion Density Study

A study of the ion density in the decaying plasma was made by measuring the Stark broadening of the first three emission lines of the hydrogen Balmer series.[20] The line width is roughly proportional to $n_i^{2/3}$, and thus provides a measure of ion density. The density measured in this way was found to decay from an initial value of 5×10^{15} cm^{-3} at the time of crowbar to a value of 2×10^{15} cm^{-3} at 250 μsec.

The broadening of emission lines of hydrogen depends upon the well known Stark effect, in which the energy levels of a radiating atom are perturbed by an externally applied electric field, resulting in a small shift in the radiation frequency. In a plasma the radiating atoms are

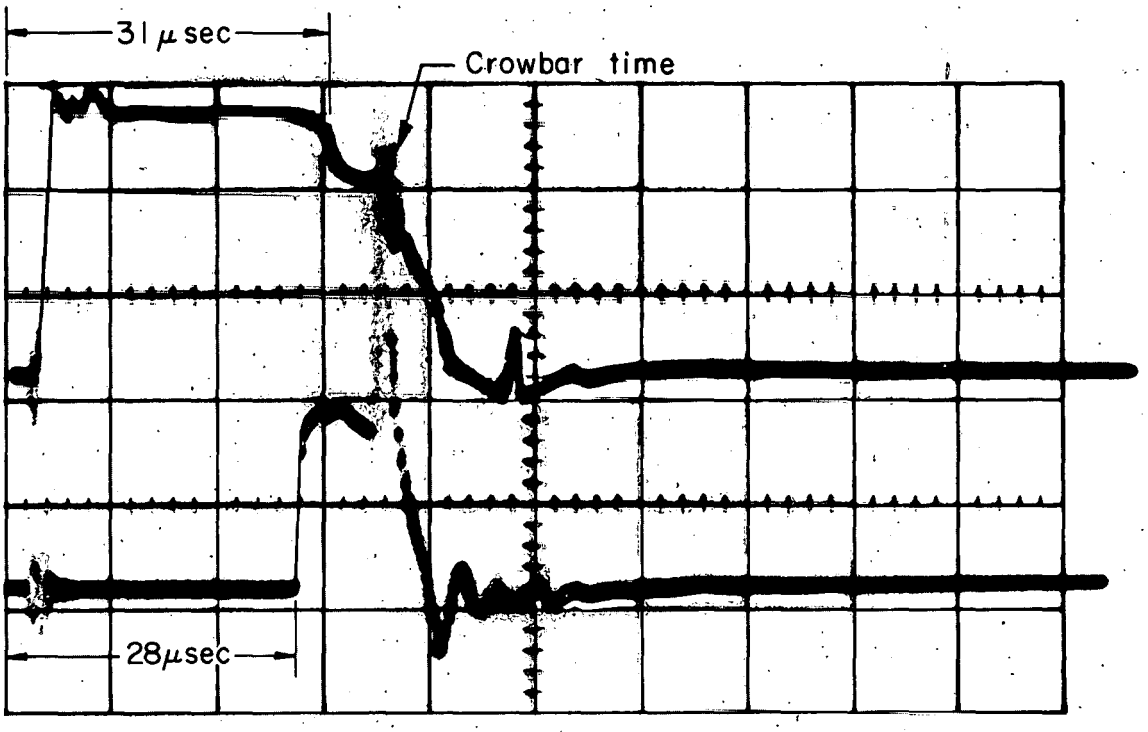

ZN-2493

Fig. 8. Oscilloscope traces showing arrival of ionization front. The top trace is the voltage on the driving coaxial electrode at 1000 v/cm; the bottom trace is the voltage on the receiving coaxial electrode at 1000 v/cm. The horizontal scale is 10 μsec/cm. The axial magnetic field is 10 kgauss. The abrupt rise of the received voltage is evidence for a well-defined ionization front. Note that the information that the front has reached the load at the receiving end (0.33 ohms, not shown in Fig. 1) requires one Alfvén transit time (2.8 μsec) to reach the driving end, at which time the driving voltage decreases somewhat.

continually being perturbed by the coulomb fields of neighboring ions and electrons. Hydrogen exhibits a first-order Stark effect in which the frequency shift is proportional to the first power of the perturbing electric field. The problem is treated statistically by taking weighted averages over all possible perturber configurations. The result is that the emission line is broadened, with the half-width of the line being roughly proportional to $n_i^{2/3}$, where n_i is the ion density. This problem was first treated by J. Holtsmark in 1919.[21] More recently a detailed calculation of the line shape has been made by Griem, Kolb and Shen, who take into account the effects of electrons as well as those of ions on the radiating atoms.[22] Inclusion of electronic effects introduces a temperature dependence into the line shapes, but the dependence is weak, and a very rough knowledge of the temperature allows the curves to be used for ion-density determination.

The ion density varies with time, so it is desirable to make a time-resolved measurement. A Jarrell-Ash model 82-000 monochromator with a resolving power of 0.22 to 0.59 Å (depending on the entrance and exit slits used, which in turn depended upon the light intensity) was used to look at a column of light 5 cm in diameter, coaxial with the axis of the tube. A photomultiplier tube at the exit slit monitored the light intensity, and its output was displayed on an oscilloscope. Traces of intensity vs time were obtained at ten different places on the line profile, and cross plots gave the line shape as a function of time. Since the light output is not exactly reproducible, (RMS fluctuation is about 20%) six or eight shots were averaged to get each point on the curves. The results were plotted and then fitted by eye to the curves of Griem, Kolb and Shen. Sample curves for H_α, H_β and H_γ are shown in Figs. 9, 10, and 11. On the H_β curve we have shown theoretical curves for ion densities differing by 1×10^{15} cm^{-3} from the best fit, to indicate the precision of the method. Also included are sample curves showing the effect on theory of varying the temperature by factors of 2.

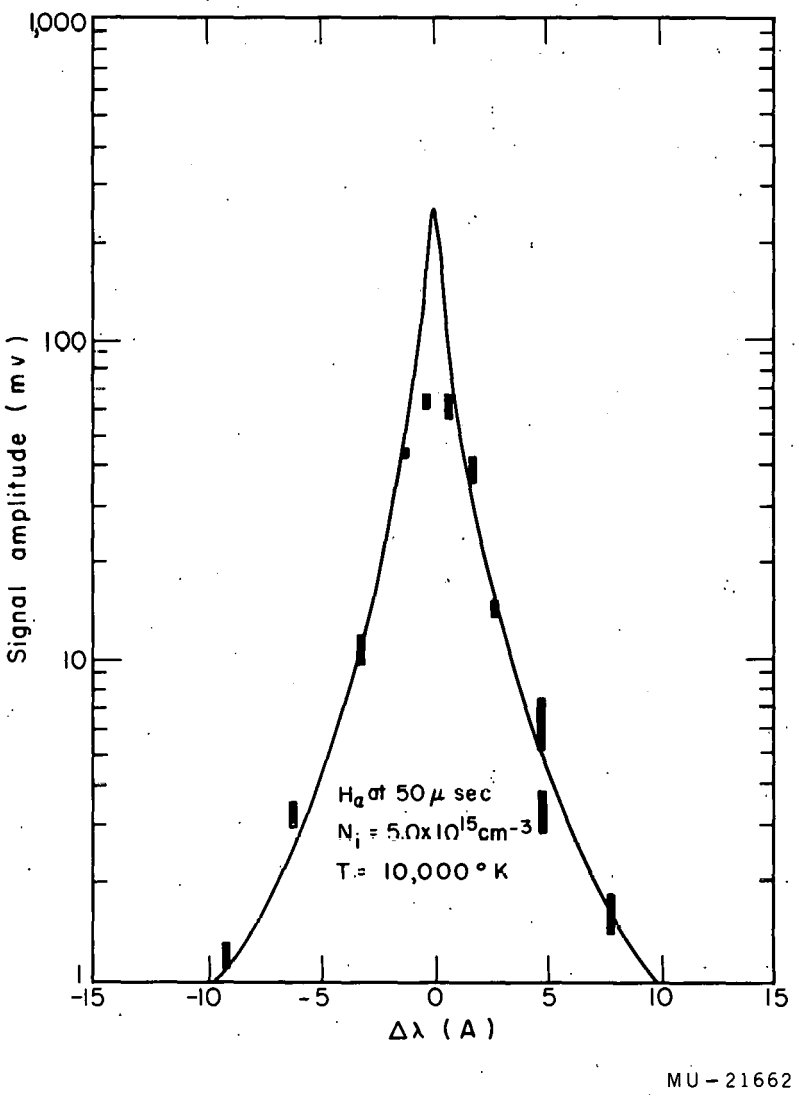

Fig. 9. H_α profile 50 μsec after the discharge was initiated. The solid curve is a theoretical profile computed for $N_i = 5.0 \times 10^{15}$ cm^{-3} and $T = 10^4$ °K.

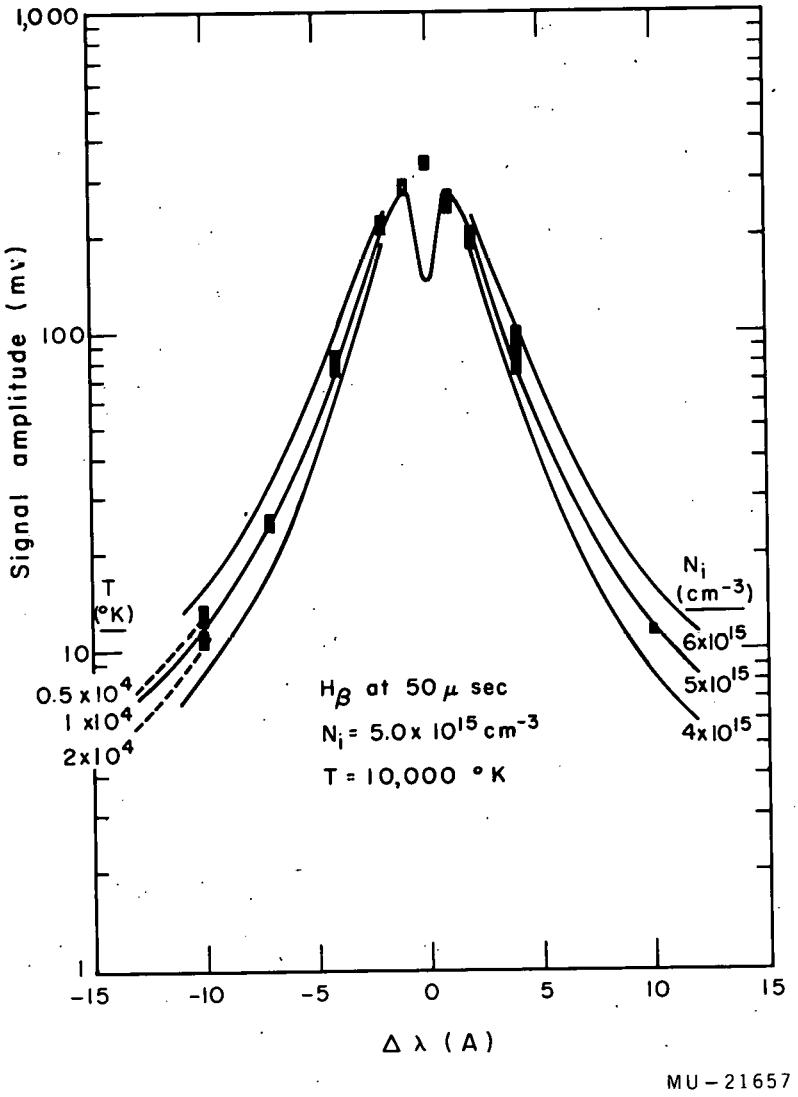

Fig. 10. H_β profile 50 μsec after the discharge was initiated. The solid curves are theoretical profiles computed for $N_i = 4.0 \times 10^{15}$, 5.0×10^{15} and 6×10^{15} cm^{-3}, at $T = 10^4$ °K. The curves are arbitrarily normalized at the peak, and are drawn to indicate the precision of fit to the data. On the left side, the effect of temperature variations by factors of 2 from 10^4 °K is indicated.

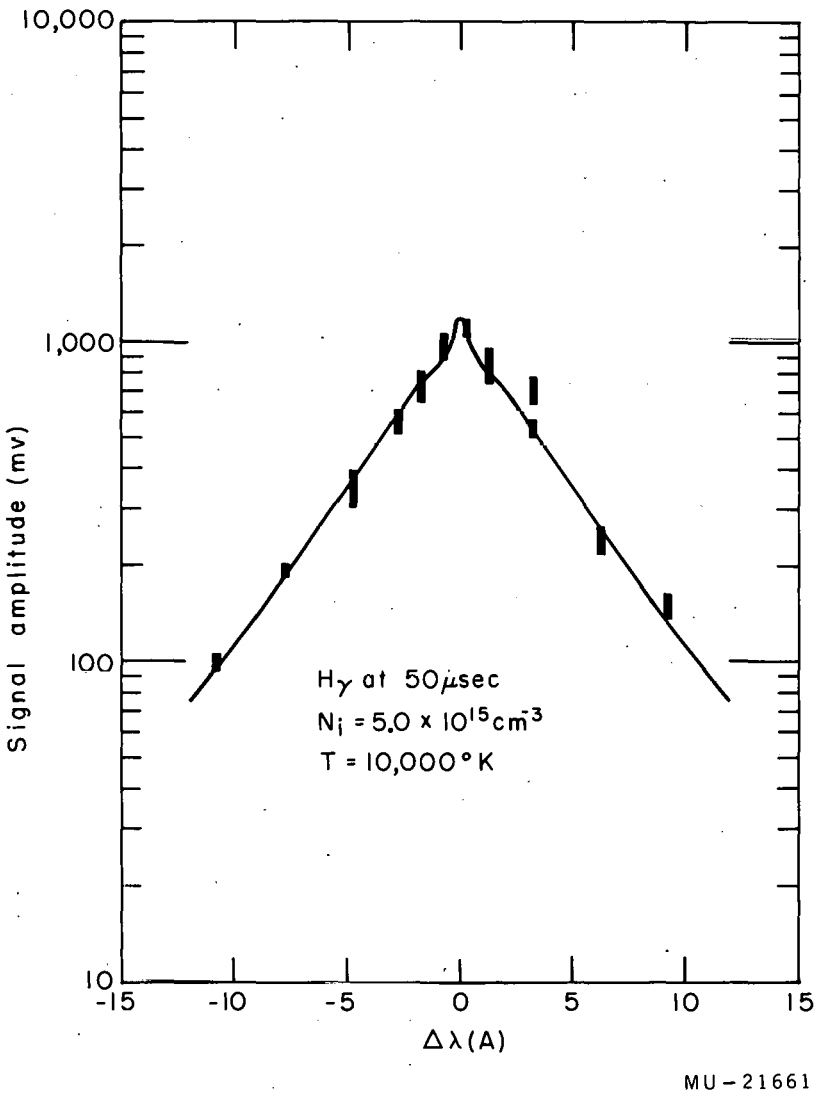

Fig. 11. H_γ profile 50 μsec after the discharge was initiated. The solid curve is a theoretical profile computed for $N_i = 5.0 \times 10^{15}$ cm^{-3} and $T = 10^4$ °K.

The ion density as a function of time as obtained in this way is displayed in Fig. 12. Two curves have been fitted to the data as aids in extrapolation to the time of crowbar. The solid curve is proportional to $\frac{1}{1+at}$ and is the curve to be expected if the decay is due to simple radiative recombination at constant temperature. The dashed curve assumes an exponential decay rate, which would result if the decay were by the lowest mode of ambipolar diffusion. The data do not distinguish between the curves, but since estimates of radial and longitudinal diffusion times lead to decay times of the order of milliseconds, it is most likely that the decay is by a volume recombination process.

Extrapolation of these curves to the time of crowbar gives ion densities at that time of 7.1×10^{15} cm^{-3} for the solid curve and 5.6×10^{15} cm^{-3} for the dashed curve. If the gas initially in the tube (100 μ) were completely ionized, we would expect an ion density of 6.6×10^{15} cm^{-3}. The data therefore indicate that the ion density is >85% of the density of gas initially in the tube. At the time the wave experiments are usually done (15 μsec after crowbar) the ion density is 5.0×10^{15} $\pm$ 1.0×10^{15} cm^{-3}.

2. Resistivity Measurement

To compare the experimentally determined attenuation of the waves with theory, it is necessary to obtain a measurement of the plasma resistivity. One approach to such a measurement would be to make a spectroscopic determination of the temperature of the plasma, calculating the resistivity by using the well-known formula of Spitzer.[11] Unfortunately, however, spectroscopic measurements of temperature are difficult at best in the temperature and density range with which we are concerned. A simpler approach is to attempt to measure the resistivity directly, by observing the potential drop produced by a known current in the plasma.

To perform this experiment, the insulator at the receiving end of the tube was provided with an electrode of the same diameter as that at the driving end, and the plasma was then prepared as described earlier,

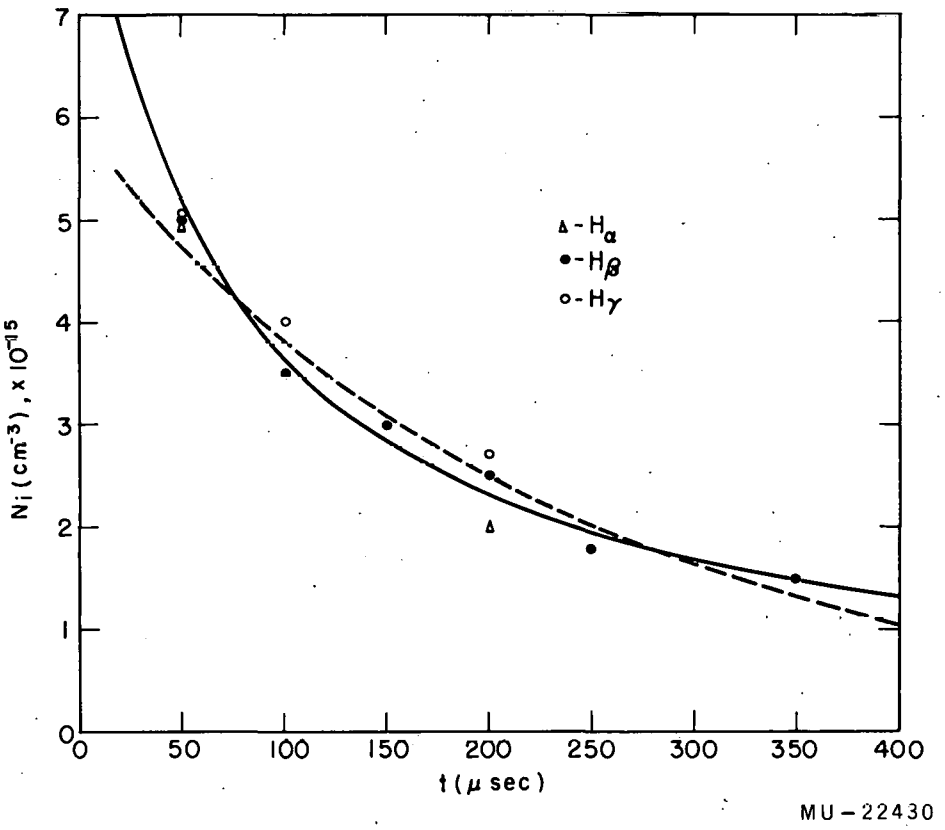

Fig. 12. The observed time dependence of the ion density. Errors (not shown) in the experimental points are estimated to be $\pm 0.7 \times 10^{15}$ cm^{-3} early in the decay period, increasing to about $\pm 1.0 \times 10^{15}$ cm^{-3} late in the decay period. The solid line is a least-squares fit, assuming the decay rate to be proportional to the square of the ion density. The dashed line assumes an exponential decay.

with B_0 = 16 kgauss and $\rho_0 = 10^{-8}$ g/cm^3. After the ionizing current was crowbarred, a small probing current was induced between the two electrodes. This current is confined to a cylinder along the axis of the tube defined by the diameter of the electrodes, since any radial currents would accelerate the plasma azimuthally, setting up a back emf that opposes such current flow. Since there is of necessity a small potential gradient along the axis of the tube (indeed, this is what we are measuring), there is also a small amount of plasma rotation. The radial current required to maintain this rotation against viscous losses constitutes a leakage current. Measurements were made under conditions where this was a small effect.

The probing current should be small enough so that the energy deposited in the plasma during the measurement does not change the average energy of the plasma. In practice, this perturbation energy was < 10% of the plasma thermal energy.

Wave observations (see Sec. IV-d, Radial Distribution of b_θ Field) have indicated that near the tube walls an insulating boundary layer tends to form that isolates the plasma electrically from the wall. This boundary layer is presumably due to a local drop in the electron temperature, and hence conductivity, near the wall. Such a boundary layer at the electrodes would add a spurious resistance to that of the main body of plasma, resulting in a high value for the calculated resistivity. Thus the measurement sets an upper limit to resistivity and a lower limit to temperature.

Equation (2.58) shows that the wave attenuation is principally determined by $\eta_{\parallel}$, which is the part of the resistivity tensor that is measured by this method. The resistivity was determined as a function of time by turning on the probing current at various times after crowbar. The results of the measurements are plotted in Fig. 13, where the indicated temperature is calculated from Spitzer's[11] formula for $\eta_{\parallel}$.

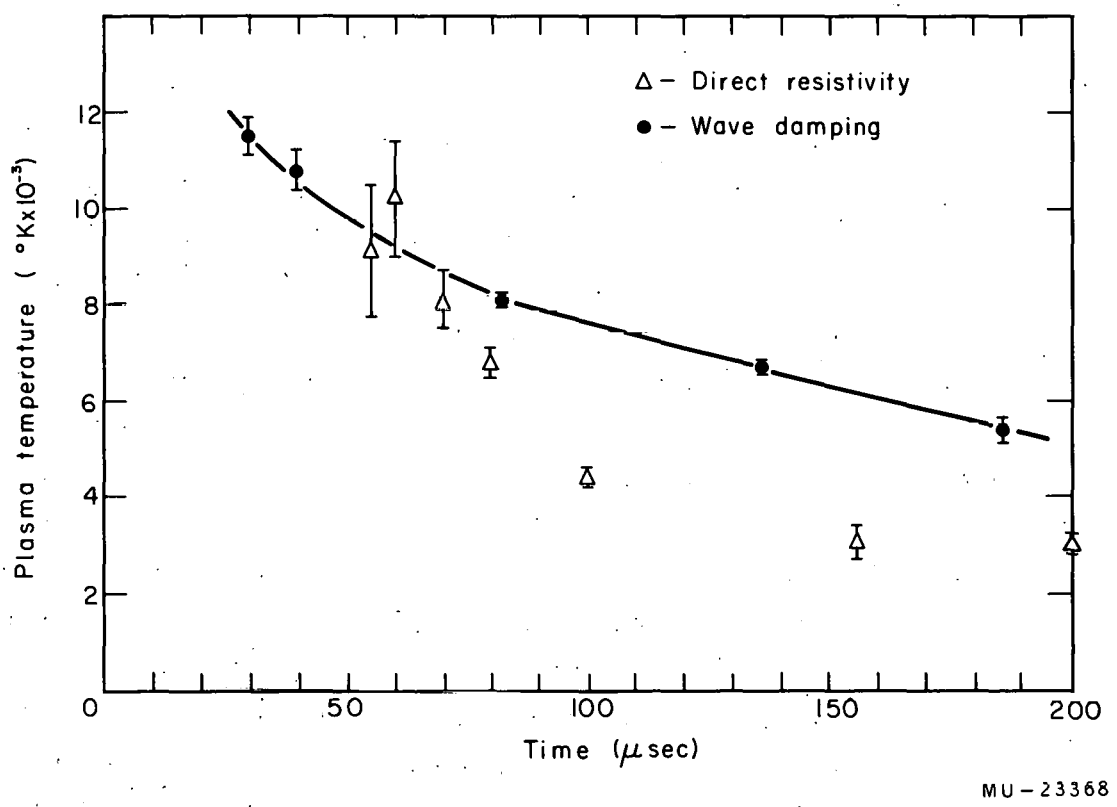

Fig. 13. The time-dependence of temperature of the decaying plasma, as determined by hydromagnetic wave attenuation and by direct resistivity measurements. The vertical bars indicate the standard deviation of the mean of a number of measurements (usually 6).

3. Impurity Levels

To compare the results of experiment with theory requires a knowledge of the mass density of gas within the cylinder. Because the presence of an unknown amount of impurity in the gas makes comparison impossible, it is most desirable to eliminate impurity elements from the discharge region. Failing in this, the next best course of action is to determine what impurities, and in what amounts, are present.

Analysis of the visible emission spectrum of the discharge reveals, in addition to strong lines of the hydrogen Balmer series, lines characteristic of Si, Si^+, Si^{++}, Si^{+++}, O, O^+, C^+ and Na. A spectrum of the ultraviolet radiation also shows lines of neutral carbon, aluminum and copper. The time dependence of these lines has been examined as an aid in fixing the source of impurity. Silicon lines are observed to increase in intensity almost linearly with time, albeit remaining at a relatively low level, during the time the ionizing wave is traveling through the tube. If the wavefront is then allowed to strike the end plate before crowbar, the light intensity rises rapidly (in about 30 μsec) to 6 or 8 times its previous intensity, then decays with a characteristic time that varies with species (Si^+ Si^{++} or Si^{+++}) and is about 100 μsec for Si^+. If the ionizing current is crowbarred just before the wavefront strikes the end plate instead, the light intensity only increases by a factor of about 2, and decays more rapidly, in about 20 μsec.

Behavior of the oxygen light is very similar to that of silicon, except that it jumps up rapidly in the first 2 μsec of the discharge, then rises linearly to the time the wavefront arrives at the far end.

Sodium light rises linearly during the transit of the ionizing wave, and is little affected by letting the wavefront strike the insulator, suggesting a source along the wall of the tube or in the gas.

The behavior of the carbon light is unique in that it rises within 2 μsec to a practically constant level during the time the ionizing wave is moving through the gas. An increase in intensity of a factor of two or three is noted after the wavefront strikes the end plate, depending on whether the current is crowbarred before or after that time. Carbon

light decays with a characteristic time of about 40 μsec. The rapid rise early in the discharge suggests a source near the driving end-possibly associated with the O-ring vacuum seals at that end. The similar early behavior of the oxygen light suggest the same source for at least part of the oxygen light.

A linear rise in time of the impurity light intensity could indicate either a continuing erosion of the driving-end insulator, or that impurity material is being encountered all along the path of the ionizing wave, i.e., on the tube walls. Both are likely possibilities, the second because material taken from the insulators on earlier shots is likely to end up deposited on the tube walls. The comparatively rapid decay rate of impurity light when the ionizing current is crowbarred before the wavefront strikes the end of the tube indicates, that the impurity atoms only penetrate a short distance into the plasma, remaining in a region near the boundary that cools rapidly.

A very rough estimate of the absolute number density of impurity atoms within the discharge region may be made by comparing observed impurity line intensities (with a monochromator) before and after introduction of a known amount of gas containing the impurity element. Since it is not certain that all the added impurity atoms will be excited, this method at best sets an upper limit to the amount of residual impurity in the region along the tube axis at which the monochromator looks. The method was used obtain such limits for carbon and for oxygen which account, along with silicon, for the most prominent impurity lines. The result was an upper limit of 0.2 μ for carbon and 0.4 μ for oxygen (O_2). Oxygen presumably comes from outgassing, bottled gas impurity, and from insulator materials. Since silicon would only come from insulator material, (no silicone oils are used in the vacuum pumps) it is assumed that the level for oxygen represents also an upper limit for silicon. Translating these figures into mass densities we obtain as an upper limit to impurity mass density 1.5×10^{-9} g/cm^3. If we use hydrogen mass densities above 10^{-8} g/cm^3, which corresponds to hydrogen pressures above 100 μ, the additional mass due to impurity should be no greater than 15% of the mass of the hydrogen. The mass density enters

the formula for wave velocity as a square root, and so the shift in velocity due to impurities would then be of the order of 8%. These calculations assume a uniform distribution of impurity atoms throughout the discharge region. In reality, the impurities seem to originate at the walls, and estimates of diffusion times for these atoms into the central plasma region indicate that they could not penetrate significantly far in the time available. The base pressure in the tube is 0.02 μ. If we assume that this residual gas is air, then we can calculate that the density perturbation to 100 μ H_2 is only about 0.28%.

Hydrogen itself may represent an impurity, since gas which is absorbed on the walls of the tube may be released in the ionization process, increasing the density of the plasma. The fact that the spectroscopically measured ion densities agree so well with the particle density of gas initially put in the tube indicates that this process is probably not important.

4. Plasma Uniformity

Gradients in temperature and charged-and neutral-particle densities must exist within the plasma, and it is necessary to inquire as to their magnitudes and effects upon the waves. The only available direct measurements of plasma properties are those already cited, which are not local measurements but integrate over a considerable portion of the plasma.

We can appeal to theoretical analysis of the ionizing wave producing the plasma to learn something of the conditions which might be expected at the time the wave experiments are performed. Analysis of such an ionizing wave has been performed by Gross and Kunkel,[23] for the case of a plane wave propagating between parallel conducting plates. The real situation is a cylindrical geometry for which the analysis has not yet been done. However, we may be able to derive some general ideas concerning the behavior of such a wave.

The calculation provides us with an approximate value for the velocity U of the ionizing wave, in terms of which the density and

temperature ratios across the wavefront are given. This is

$$U = \frac{16}{9}\left(2\epsilon_i + \epsilon_d\right)\left[-1 + \left(1 + \left[\frac{3B_0 b_\perp}{4\mu_0 \rho(2\epsilon_i + \epsilon_d)}\right]^2\right)^{1/2}\right], \tag{3.1}$$

where ϵ_i and ϵ_d are respectively the ionization and dissociation energies per unit mass of gas, and $b_\perp$ is the transverse magnetic field due to ionizing current.

The density ratio across the front is approximately 8/5. Since the density behind the wave is greater than that in front, the gas behind must be moving in the direction of the wavefront. We denote the axial velocity of this gas by v_2. Then mass conservation shows that $v_2 = (3/8)\,U$. We define $a_\perp^2 \equiv \frac{b_\perp^2}{\mu_0 \rho}$. Then, for the case where $V^2 \gg U^2 \gg a_\perp^2$, the temperature behind the wavefront is given by

$$RT = \frac{\gamma}{(\gamma+1)^2}\left[U^2 - a_\perp^2\right], \tag{3.2}$$

where γ is here the ratio of specific heats, and R is the gas constant per unit mass.

The conditions given are only those immediately behind the ionizing wavefront. Since there is no driver piston, there must be a rarefaction wave which fills the region between the wavefront and the back insulator. The rarefaction wave has not yet been analyzed, but in general it must cause the axial velocity of the gas in this region to fall from v_2 just behind the ionizing wave to zero at the back wall. This implies that the density will also grade from a maximum just behind the ionizing wave to a minimum at the back wall. If the driving current is large enough so that the magnetic field pressure due to the current is comparable to the gas pressure behind the ionizing wave, then some of the gas may be pushed entirely clear of the back plate by a sort of snowplow effect.

The dependence of U on B_0, ρ and $b_\perp$ has been checked experimentally to establish the validity of Eq.(3.1). The agreement of the predictions of this equation with the observed velocity of the ionizing wave is within 40% in the range of parameters that were studied ($5 < B_0 < 16$ kgauss; $2\times10^{-9} < \rho < 4\times10^{-8}$ g/cm^3; $2\times10^3 < I < 6\times10^3$ amp). The agreement is probably as good as might be expected in applying this theory to a cylindrical geometry.

The model from which these theoretical results are derived postulates a perpendicular current flow in the wavefront, and no current elsewhere in the gas. The return path for current is assumed to be through conducting plates lying parallel to the static magnetic field. The calculated temperature behind the wavefront based on this model (3×10^4 °K for $\rho = 10^{-8}$ g/cm^3 and $B_0 = 16$ kgauss) must bear little relation to that in the actual case for which there exists a rarefaction wave, within which both axial and radial currents flow (the radial current maintains the plasma rotation against viscous losses, neglected in the theory). These currents are probably the principal determinants of the plasma temperature.

The chief conclusion we can draw from this analysis is that there is likely to be a considerable axial motion of the plasma behind the ionizing wave, which would result in an axial density gradient. Application of the "crowbar" halts the gas rotation, but does nothing to arrest the axial motion of the plasma.

The density gradients thus produced will smooth out in a time comparable to the time required by an acoustic wave to traverse the system. The gas temperature this early may be about 13,000 °K (see Fig. 13). This gives a sound speed $V_s = 1.34\times10^6$ cm/sec, and a transit time of 63 μsec. For the wave experiments, in order that there be low dissipation, the wave is usually introduced at about 15 μsec after the ionizing front has reached the end of the tube, so there may still exist a moderate density gradient. Experimental observation of the profiles of the Balmer lines seems to argue against any large axial density gradients, since the experimental line shapes in such case would not fit the

theory for a single density, while in practice the line shapes fit the theory very well. In any case, the existence of an axial density gradient would not affect wave measurements much, since the density enters into the Alfvén velocity only as a square root, and the hydromagnetic wave measurements necessarily give an average velocity over the length of the tube. A calculation of the error that would be made in measuring the velocity if the density graded linearly from zero at one end to twice the equilibrium value at the other end, certainly an extreme case, leads to an error of only 6% in velocity, which is of the order of other experimental errors. Measurements of attenuation and spatial distributions of fields are similarly insensitive to density variations.

The plasma left behind the ionizing wave is rotating, and under some conditions radial plasma drift will result, producing radial density gradients. A rough calculation of the magnitude of this kind of drift has been given by Baker et al.,[24] and is followed here. The radial drift velocity is obtained from Ohm's law (Eq. (2.9).

$$v_r B_0 = \eta j_\theta \tag{3.3}$$

The azimuthal current density j_θ, in the absence of pressure gradients, is obtained from the equation of motion (Eq. 2.8), where now the time derivative is assumed zero and the inertial contribution comes from the $\underset{\sim}{v} \cdot \nabla \underset{\sim}{v}$ term.) This gives

$$j_\theta = \rho \frac{v_\theta^2}{rB_0} . \tag{3.4}$$

v_θ is the azimuthal velocity of the gas, and is shown by Gross and Kunkel[23] to be approximately equal to the square root of twice the ionization potential per unit mass, e_i of the gas. We now define a quality factor Q as the ratio of the distance the plasma drifts in the radial direction to the tube radius, in the time that it takes the front to move through the tube. Let ℓ be the length of the tube, and b its radius. We will somewhat

arbitrarily take r = b. Then:

$$Q = \frac{2\eta \rho \epsilon_i \ell}{B_0^2 U b^2} . \qquad (3.5)$$

The condition that the radial density gradient be small is $Q \ll 1$.

Putting numbers characteristic of this experiment into the above expression shows that Q equals 1 at B_0 approx 2 kgauss. To avoid large radial density distributions than, B_0 is kept well above this value.

5. Temperature Gradients

The thermal conducticity coefficient κ for a hydrogen plasma as given by Spitzer[11] is proportional to $T^{5/2}$. This strong dependence on temperature provides a rather remarkable mechanism for leveling out temperature gradients and maintaining a uniform temperature in the plasma. Near the walls, the plasma must cool by thermal conduction. The thermal conductivity drops as a result, reducing further heat flow to the walls. Thus the plasma acts like a "heat switch," maintaining the temperature within the body of the plasma.

The conservation equation $\frac{dW}{dt} - \nabla \cdot \kappa \nabla T = 0$ that describes the flow of heat may be used to estimate the rate of cooling by thermal conduction to the walls. (W is the thermal energy density) The dependence of κ on temperature renders the equation nonlinear; however it is possible for a case in which the heat flow is assumed to be purely radial to obtain a similarity solution which indicates the cooling rate. The details of the calculation are given in Appendix C. For an initial temperature distribution that is nearly flat in the central portion of the tube (see Fig. 26), and which then falls rapidly to room temperature at the walls, the temperature at the center will drop from 12,000 ^{o}K to 9,000 ^{o}K in about 320 μsec. This calculation ignores the effects of particle diffusion to the walls. An estimate of the rate of diffusion of a plasma at 10^4 ^{o}K across

a magnetic field of 16 kgauss indicates that the time taken to diffuse one tube radius is about 25 msec.

Diffusion axially to the ends of the tube is controlled by the rate of diffusion of ions into the neutral atoms returning from the end, for which the dominant process is the charge exchange collision. A rough calculation gives 16 msec as the time for ions to diffuse one half the length of the tube. These decay times are both long compared to the time obtained from the thermal conductivity calculation, indicating that energy transport to the walls is determined mostly by thermal conduction. These estimates greatly over-simplify the problem, but are probably sufficient to indicate the order of magnitude of the effects.

6. Energy Balance

The power delivered by the pulse line during ionization is almost constant. Under the typical operating condition where B_0 = 16 kgauss and the mass density is 1.10×10^{-8} g/cm^3, the energy delivered to the tube during breakdown is about 760 joules. This energy goes into dissociation and ionization of the gas, ohmic plasma heating, kinetic energy of rotation of plasma (due to $\underset{\sim}{j} \times \underset{\sim}{B}_0$ forces) viscous losses arising from rotation, and radiation. It is instructive to try to account for these energies quantitatively. As pointed out before, ion density measurements show that the ion density before crowbar is probably $> 6 \times 10^{15}$ cm^{-3}, and temperature measurements indicate a temperature of around 13,000 ^{o}K. The energy required to ionize and heat the plasma to this extent is 234 joules. The kinetic energy of rotation is obtained by measuring the charge flowing out of the tube after crowbar, which is a measure of the stored energy. This proves to give 154 joules. Viscous losses due to radial shear may be estimated by measuring the average radial current to the tube wall in the region behind the ionizing front. This is the current required to maintain the plasma rotation against viscous and other losses, and requires 170 joules. A calculation of the radiation to be expected from the tube indicates that this is a negligible energy loss. Thus we can fairly definitely account for 558 joules out of 760. An

analysis of the viscous losses in a rotating plasma has been made by Baker et al.,[24] indicating that losses due to axial shear at the end plates should dominate over other viscous effects. It was not possible to measure the current flowing along the end plate, so we can only speculate that some of the remaining energy goes into viscous losses there.

7. Summary of Plasma Properties

The ionizing wave produces a plasma that is initially almost fully ionized – the percent ionization is certainly greater than 85% – and whose ion density decays by a factor of 2 in about 150 μsec. The temperature immediately behind the ionizing wave may be as high as $3\times10^4\ ^oK$ (from Eq. (3.2)), and is measured to be about $1.2\times10^4\ ^oK$ 20 μsec after crowbar. The temperature decreases by a factor of 2 in about 150 μsec, probable loss mechanisms being thermal diffusion to the walls and radiation. These decay times are all large when compared to the time required for an Alfvén wave to traverse the system, so during any given measurement the plasma condition is essentially uniform.

During the discharge there is an influx of impurity atoms into the plasma, most of them originating at the tube walls. Diffusion times are slow, so the main body of the plasma is relatively free of impurity atoms while the wave experiments are performed. The plasma probably has an axial density gradient, which does not greatly affect the observable wave properties. Radial density gradients may be minimized by proper choice of operating parameters – high magnetic field and low density.

We are led by these results to place some limits on the variation of experimental parameters. Considerations of plasma uniformity as well as low dissipation (for waves) indicate that high axial magnetic fields of >10 kgauss are desirable. The upper limit here is of a practical nature, i.e., the availability of power to produce the field.

Plasma uniformity also demands low densities, but we are here limited by impurities — as densities become lower, the effect of impurities increases. The practical limitations of density seems to be 5×10^{-9} $g/cm^3 < \rho < 2\times10^{-8}$ g/cm^3. Some extension to higher density may be realized by modifying the ionization mechanism.

Temperature changes are easily obtained in the decaying plasma, but changing the initial temperature of the plasma by any considerable amount seems to be very difficult.

IV. EXPERIMENTAL RESULTS

A. Wave velocity

The velocity of the hydromagnetic waves has been measured under a variety of combinations of the parameters B_0 and ρ. These measurements are complicated by the fact that, as was noted in the section on plasma uniformity (III-4), the plasma preparation process necessarily changes when either B_0 or ρ is varied, making the interpretation of results sometimes difficult.

These measurements were generally made using a single-pulse wave. A Fourier analysis of this pulse shows that it includes frequencies from zero up to about $\omega = 10^7$ sec^{-1}. Since, according to the theory developed in Sec. II, frequencies below $\omega = 10^6$ sec^{-1} suffer a dispersion in velocity, the shape of the pulse must change with time. For a symmetrical pulse, the corrections to the velocity made by making this effect into account are of order a^2 and should be negligible.[24A]

The density may be varied in a fairly straightforward way, but only by a factor of two, by replacing the hydrogen gas by deuterium. In principle, this has some advantage over just increasing the hydrogen particle density since the energy required for ionization and dissociation is not changed. In practice the difference was not noticeable. The results of velocity measurements for various densities of hydrogen and deuterium are presented in Fig. 14. The theoretical curves are calculated on the assumption that the density to be used is the total mass density of the gas initially put into the tube. Thus we assume strong coupling, so that any neutrals present move essentially with the ions. The observed velocities are generally high, indicating that the density may have been lower than expected. There are two possible explanations for the discrepancy. The assumption of strong coupling may not be valid, so that the velocity we measure is really determined by the ion density alone, while on the other hand there may actually be a lower

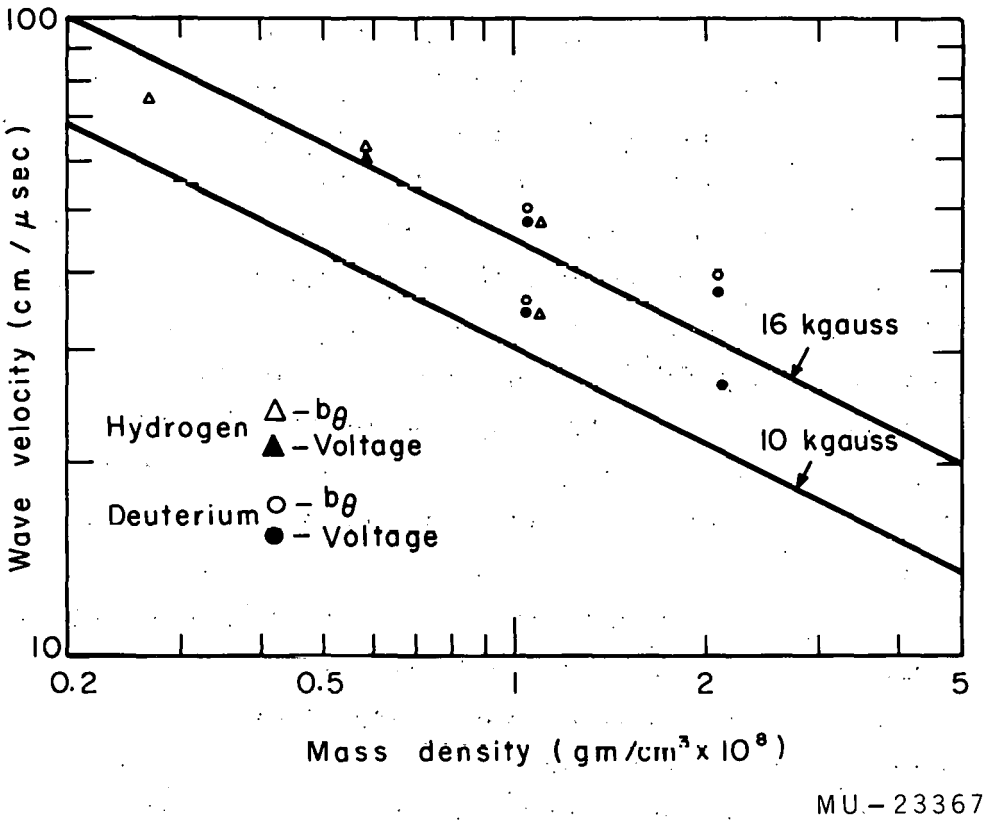

Fig. 14. Wave velocity as a function of mass density for hydrogen and deuterium. The theoretical lines are calculated assuming participation of both ions and neutrals in the wave motion. The size of the dots gives roughly the standard deviation of the mean of six or more measurements.

total density in the discharge region than that predicted.

The quality factor Q associated with radial drift of the plasma is about 0.015 in this case, so the effects of such drift should be negligible, although perhaps this effect should not be ruled out altogether. Let us now examine the assumption of strong coupling. In the section on theory we showed that the Alfvén velocity for the case of strong coupling between ions and neutrals should depend upon the total mass density-ions plus neutrals. In order to check this result, the wave velocity was measured as a function of time in the decaying plasma. The curves of Fig. 15 show the measured velocity plotted as a function of the spectroscopically determined ion density. The experimental results fall in between the theoretical predictions for strong coupling ($\rho = \rho_i + \rho_n$) and for weak coupling ($\rho = \rho_i$).

In Appendix A it is shown that coupling is strong if $\tau = \omega/\nu_{ni}$ is small compared to unity. ν_{ni} is the collision frequency per particle for neutrals, and is approximately equal to $n_i \sigma_{ni} v_T$ where σ_{ni} is the neutral-ion charge-exchange cross section and v_T is the average thermal velocity of neutrals. The charge-exchange cross section has only been measured for particle energies above 100 ev.[25] However, in the energy range where it has been measured it falls fairly uniformly 20% above the theoretical calculations of Dalgarno and Yadov.[26] Somewhat arbitrarily applying this 20% correction to the theory of Dalgarno and Yadov at 1 ev, the approximate temperature of the plasma, we find $\sigma_{ni} = 5.7 \times 10^{-15}$ cm^2. Using this figure we then obtain $\nu_{ni} \approx 5 \times 10^7$ sec^{-1} and τ approx 0.1. This is only a marginal case of strong coupling, particularly considering the uncertainty in the charge exchange cross section, so the results of Fig. 15 are perhaps not surprising. If an accurate determination of the temperature of the plasma can be obtained, it should be possible to use such measurements of wave velocities to determine the low-energy charge-exchange cross section.

Owing to the necessity to keep the quality factor Q small, the velocity could not be checked at low B_0 using the method of ionization already described. The measurements of wave velocity at higher axial fields are presented as a function of axial magnetic field in Fig. 16.

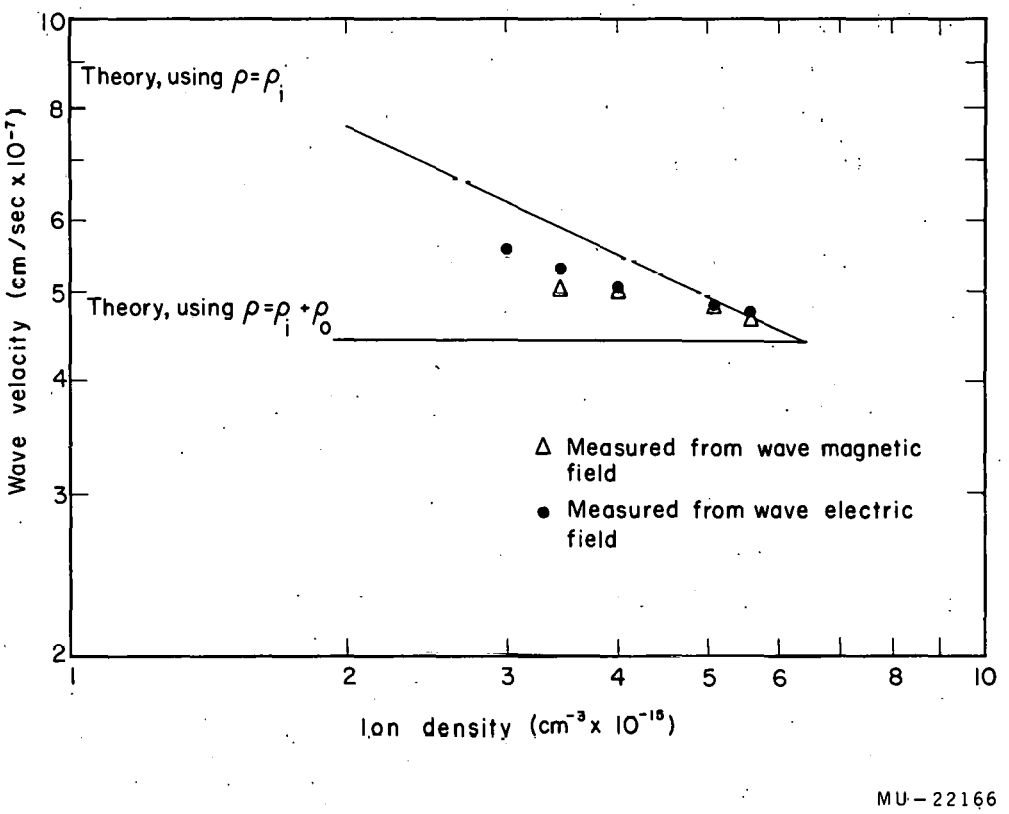

Fig. 15. Alfvén wave velocity vs spectroscopically determined ion density. These measurements were made in the decaying plasma by inducing the wave at various time delays after the plasma started to decay. Axial magnetic field strength 16.0 kgauss, $\rho=10^{-8}$ g/cm^3.

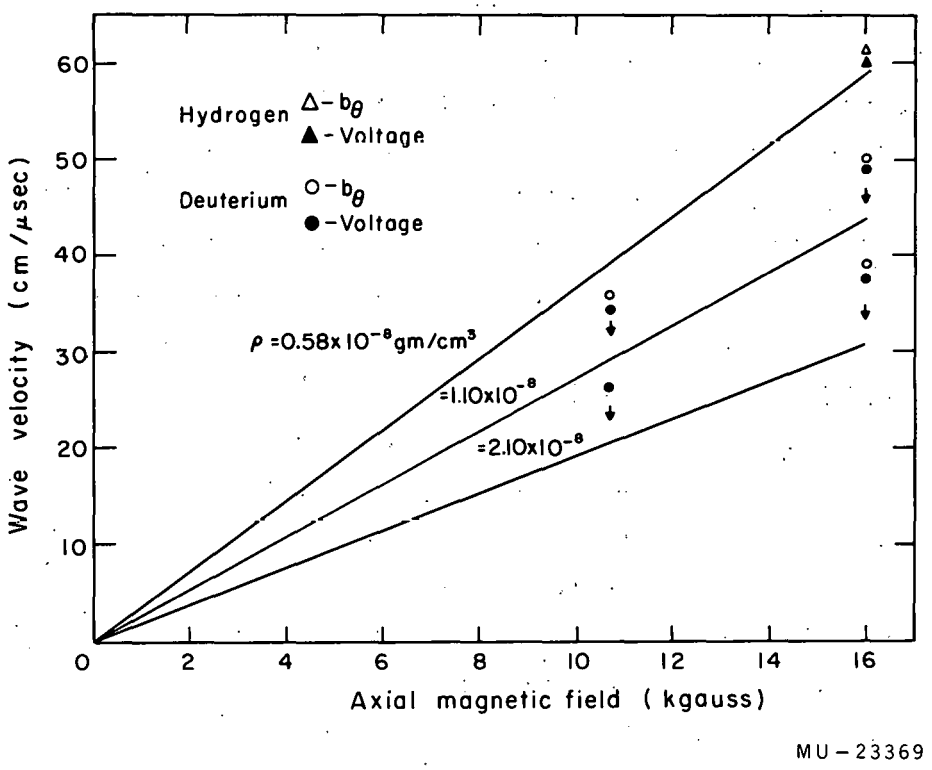

Fig. 16. Wave velocity as a function of axial magnetic field strength at various mass densities. Ionization current induced at one end. The size of the dots gives roughly the standard deviation of the mean of six or more measurements.

A different method of plasma preparation has been used, in which the energy storage bank was discharged between electrodes mounted at opposite ends of the tube. Ionizing current in this case was sinusoidal, with a period of 65 μsec and a peak value of 3×10^4 amp. Wave measurements were then made at 65 μsec when the current was passing through zero. Under these conditions, the ionization mechanism probably consists of two ionizing waves that converge to the center of the tube, automatically self-crowbarring the plasma rotation when they meet. After they meet, the externally applied current just flows axially through the tube, mostly confined to the cylindrical region defined by the diameter of the central electrodes. The current to the ionizing waves is greater than in the ionization mechanism previously discussed, so radial particle diffusion effects should be reduced (cf. Eq. 3.5). The high axial current density must tend to set up a large radial temperature gradient, which is opposed by the effect of a high thermal conductivity. Estimates of the rates seem to indicate that the radial gradient at the time the wave is induced will be somewhat higher than in the previously discussed case. Axial flow velocities are higher with this method of ionization, but the resulting axial density gradient occurs over a shorter distance and is allowed more time to smooth out. The additional time available for impurity penetration does not seem to be significant, since the measured wave velocity was the same whether measured at 30 μsec or at 90 μsec.

The results of this velocity measurement, extended to axial field strengths of 5 kgauss, are presented in Fig. 17. Agreement with theory is generally very good.

B. Attenuation

The attenuation constant for the wave is given in Eq. (2.58). It consists of two parts—that produced by ohmic damping within the body of the plasma, and that due to the presence of neutral particles. An estimate of the damping which might be expected from viscous losses[27] in the plasma indicates that this process is negligible compared with the aforementioned ones. In general, the attenuation of waves in

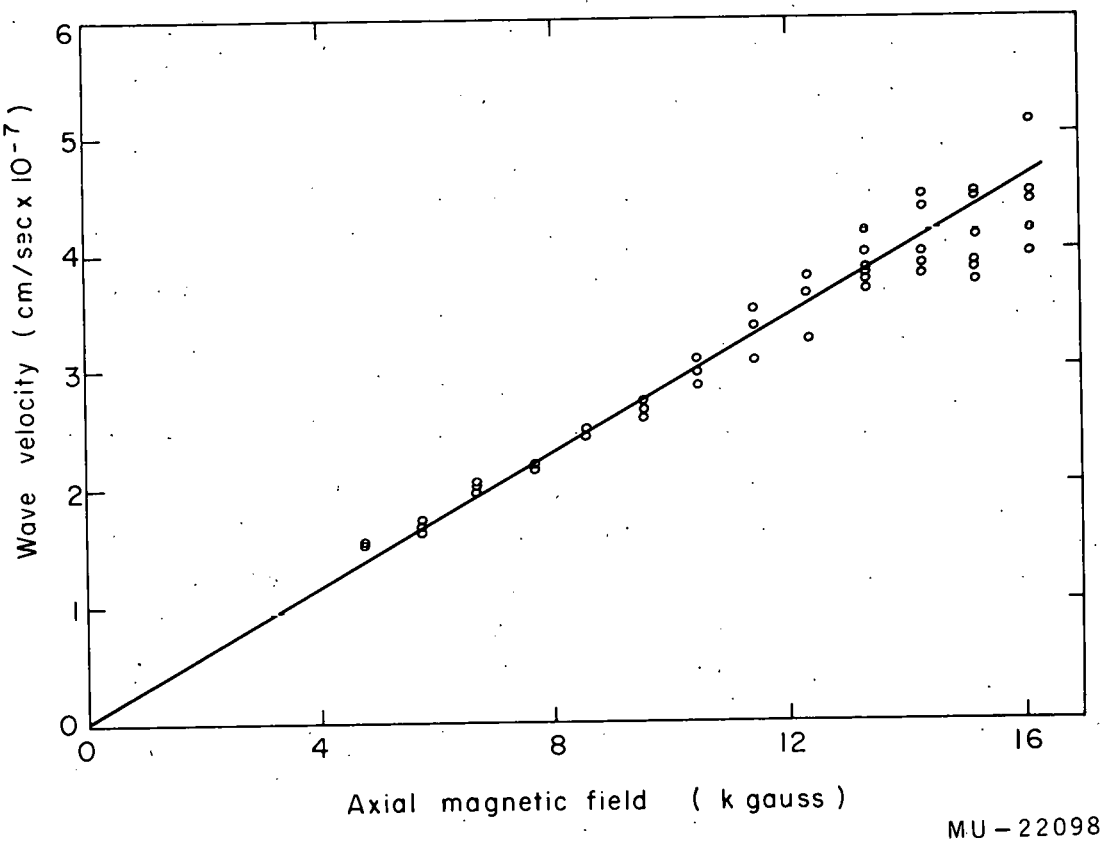

Fig. 17. Wave velocity as a function of axial magnetic field strength, $\rho = 10^{-8}$ gm/cm^3. Ionization current is axial from an electrode at one end to a similar electrode at the other end.

this experiment is high–the waves typically have a damping length which is only two or three times the wavelength. Hence, the studies of attenuation were necessarily done at high magnetic fields, where damping is lowest. Under these conditions, $\omega^2/V^2 \approx 100\ M^{-2}$ and $k_c^2 \approx 3000\ M^{-2}$, so the ω^2/V^2 term is ignored in the ohmic damping constant ϵ_j. Both ϵ_j and ϵ_n are inversely proportional to V and hence to B_0, so it is in principle not possible to distinguish between them by making measurements at various values of axial field strength. Unfortunately, making B_0 small enough so that the ω^2/V^2 term becomes important causes the attenuation to be too high for good measurements.

The attenuation constant depends strongly on the two variables B (through V) and η, the resistivity. Since the resistivity is a strong function of temperature, and the temperature falls with time in the decaying plasma, the attenuation may be measured at different temperatures merely by inducing the wave later and later after crowbar. The direct resistivity measurements described in the section on plasma preparation (III-D) provide us with a means for checking the damping measurements. The results of measuring the plasma resistivity as a function of time after crowbar, using both methods, are presented in Fig. 13. Both measurements tend to put upper limits on the resistivity and hence lower limits on the temperature. The excellent agreement between the two determinations of resistivity early in time lends support to the notion that both are really measures of the same effect. The difference in observed resistivity later in time is probably due to the development of a cool, relatively high resistance boundary layer at the electrode surfaces. Such a layer would not affect the wave measurements since current densities are high enough to heat the layer locally, reducing its resistivity.

The attenuation has also been measured as a function of axial magnetic field B_0. In Eq. (2.58) we showed that the attenuation constant ϵ should depend on the inverse first power of axial field strength.

Measurements were made using the end-to-end ionization procedure described in the previous section, since this should have resulted in minimizing the dependence of plasma conditions on axial field strength. The results of the measurement are presented in Fig. 18. The scatter in the experimental points is probably due to shot-to-shot temperature variations in the plasma, and to the observed presence of $m \neq 0$ modes (see Sec. IV-E, Auxiliary Checks).

C. Reflections

An important check on the theoretical predictions for the wave fields is provided by the observation of wave reflections. Reflections have been observed to occur from insulating boundaries, conducting boundaries, and from a plasma-neutral gas interface.[28] In all cases, the observed change of phase of the wave fields on reflection has been in agreement with theory.

The fields easily accessible to measurement are the magnetic field b_θ, measured by probes in the plasma, and the radial electric field, which we measure as $V = \int_a^b E_r \, dr$, the voltage across the end electrodes.

At an insulating boundary, represented by a pyrex end plate, the axial current density j_z associated with the wave must be zero. Reference to Eq. (2.48) for $j_z(r, \ell)$ then shows that $C_n' = - C_n$, where we use the prime to denote quantities associated with the reflected wave. The reflected wave travels in the negative z direction, so $p_n' = - p_n$. Equation (2.43) then shows that b_θ reflects out of phase by 180 deg, and Eq. (2.52) shows that E_r reflects in phase. Similar considerations for a conducting boundary, characterized by $E_r(r, \ell) = 0$ reveal that in this case the situation is reversed—b_θ reflects in phase and E_r reflects 180 deg out of phase.

Observations were made using a single pulse, so that the reflections would be easily seen. Figure 19 shows oscillograph traces of b_θ and V for the case of reflection from a pyrex end plate. The upper trace is the voltage measured at the driving end of the tube.

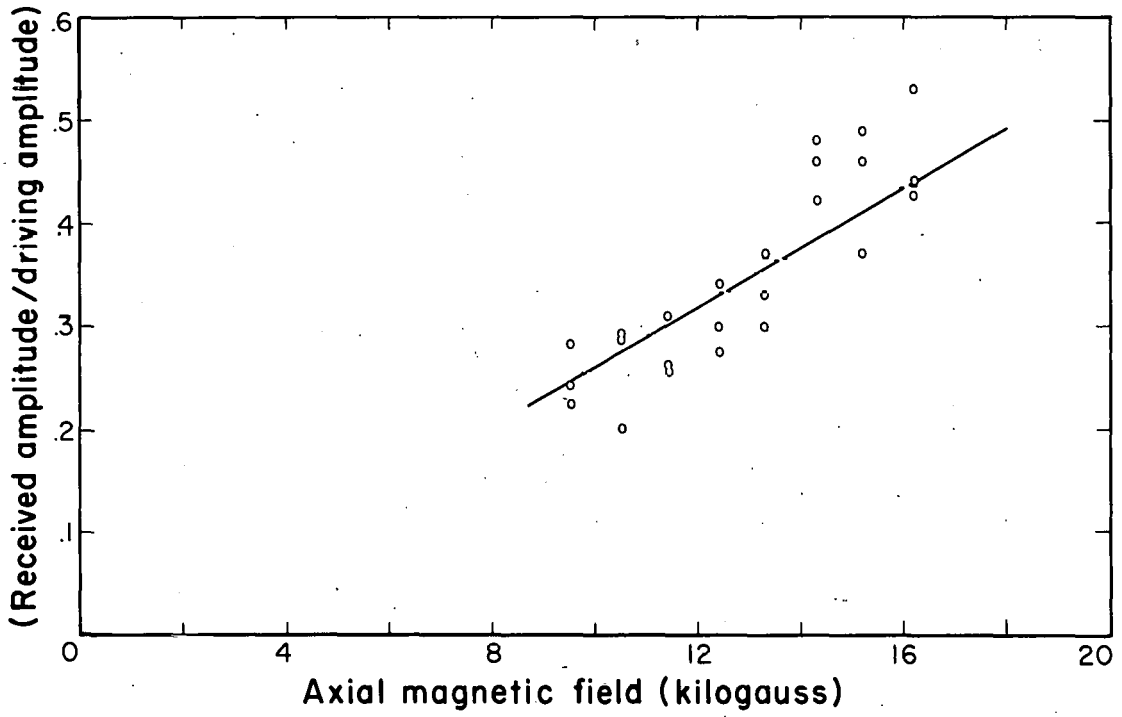

MU-18261

Fig. 18. Attenuation measured as a function of axial field strength. Solid curve is a plot of the ratio receive to driving amplitude, derived from Eq. (2.58), and Normalized at 12 kgauss. Shots are plotted individually.

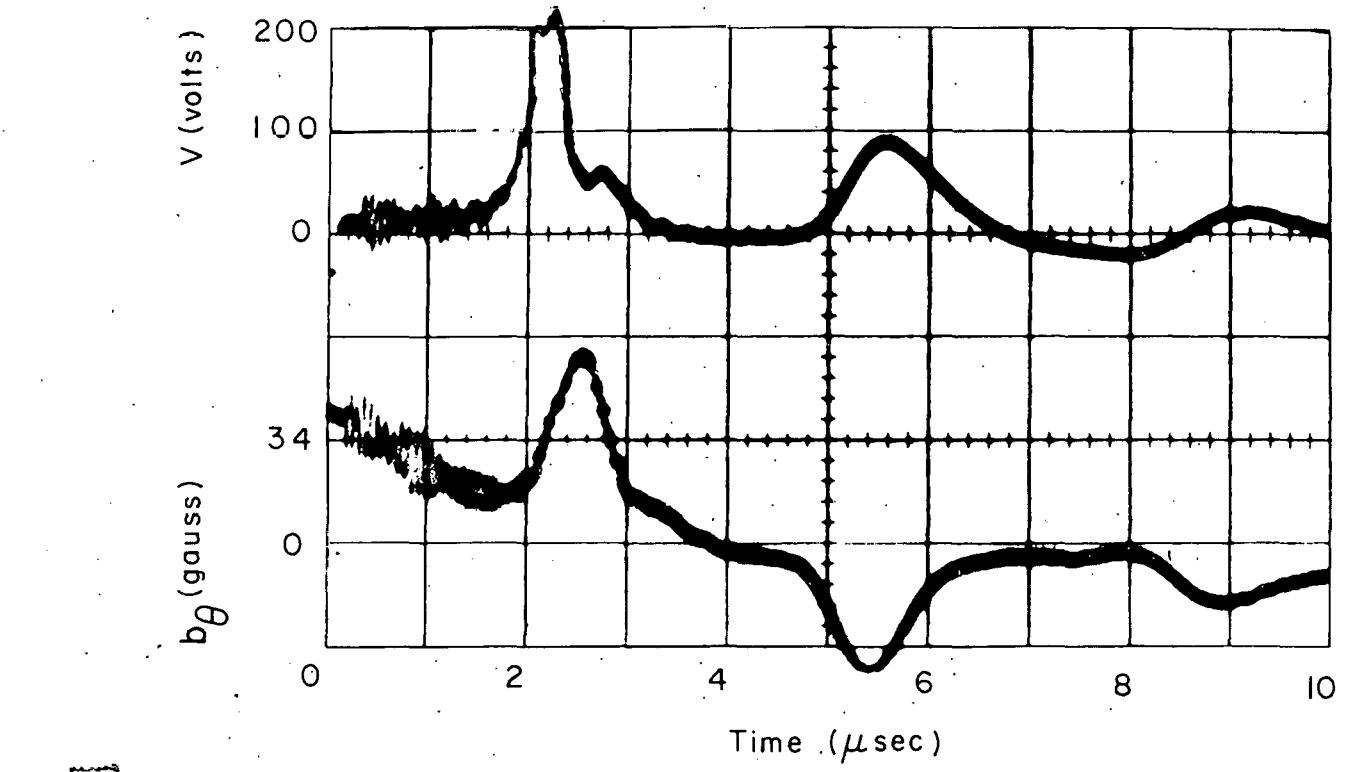

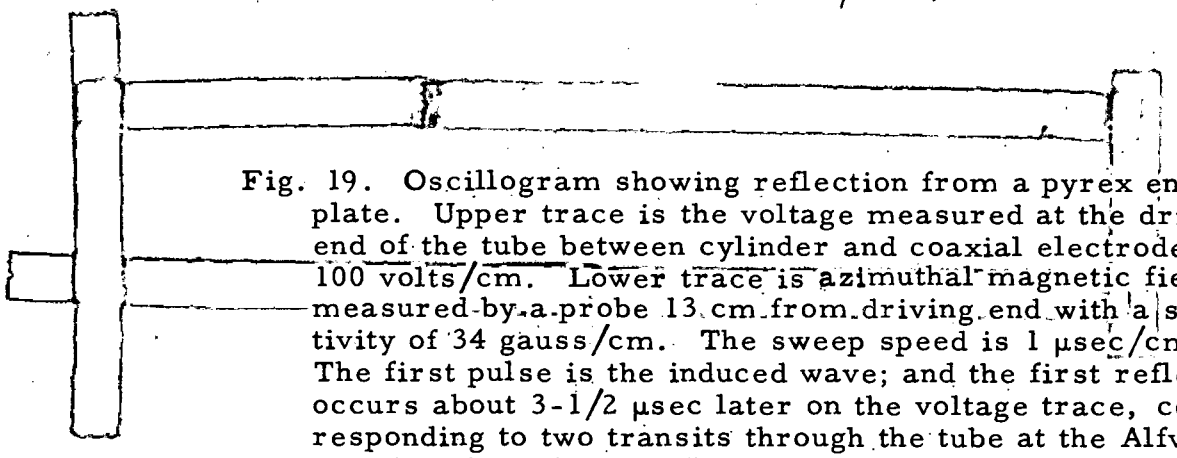

ZN-2622

Fig. 19. Oscillogram showing reflection from a pyrex end plate. Upper trace is the voltage measured at the driving end of the tube between cylinder and coaxial electrode at 100 volts/cm. Lower trace is azimuthal magnetic field, measured by a probe 13 cm from driving end with a sensitivity of 34 gauss/cm. The sweep speed is 1 μsec/cm. The first pulse is the induced wave; and the first reflection occurs about 3-1/2 μsec later on the voltage trace, corresponding to two transits through the tube at the Alfvén speed. The voltage reflects in phase, the magnetic field out of phase, in accordance with theory for a nonconducting boundary.

The first peak is the induced pulse, and at 5.6 μsec the in-phase reflection returning from the far end of the tube is seen. The lower trace shows the azimuthal magnetic field b_θ, measured by a probe 13 cm from the driving end. The reflected wave is out of phase, as predicted.

An attempt to show reflection from a copper end plate produced the unexpected result shown in Fig. 20. The phases of the reflected waves are appropriate to reflection from an insulating boundary. The resolution of this paradox is most likely found in the fact that the observations were made in a decaying plasma. The tube wall is, in effect, a low-temperature heat sink, and the plasma near the wall must cool by thermal conduction. Since the electrical resistivity is a strong function of temperature, the resistivity near the wall becomes high, accounting for the insulating-boundary type of reflection. If this hypothesis is correct, it might be expected that a high-density current flowing through the plasma to the wall and maintained by an external source would provide electrical contact between the plasma and the wall. The ionizing current can perform just such a function, since if it is not crowbarred after it has filled the tube with plasma, the current will just flow axially through the tube to the end plate. The wave was therefore induced while this current was flowing, and the reflections appropriate to a conducting boundary shown in Fig. 21 were obtained.

Finally, an attempt was made to reflect a wave from the ionizing wavefront as it was moving through the tube. Since during this time background noise on both b_θ and V is high, the ionizing current was crowbarred while the ionizing wavefront was about half way through the tube. Plasma pressure causes a shock to continue on after the current is gone, but this gasdynamic shock travels considerably slower than the electrically driven ionizing wave. The hydromagnetic wave was induced about 15 μsec after crowbar. The observed reflections from the interface thus produced are shown in Fig. 22. The current was crowbarred just as the ionizing wave reached a point 58 cm from the driving end of the tube. Using the observed reflection time and the wave velocity as

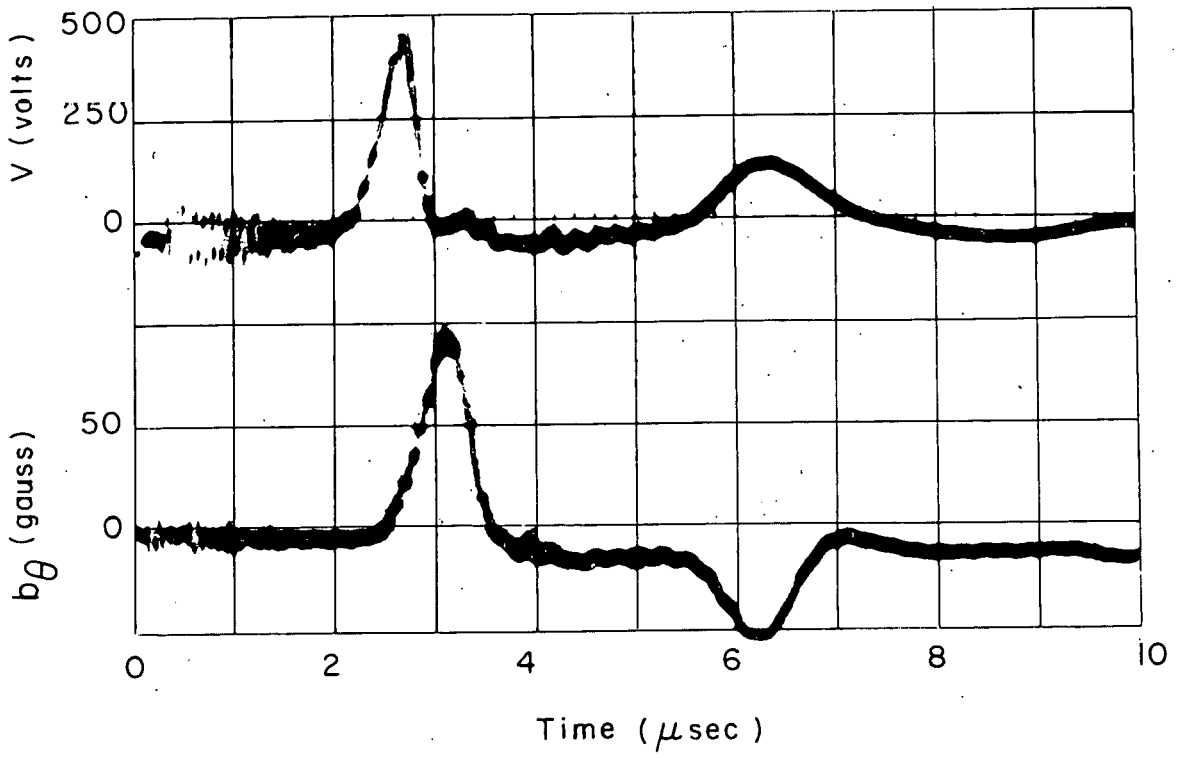

ZN-2623

Fig. 20. Oscillogram showing reflection from a copper plate 30 μsec after plasma has started to decay. Traces are as in Fig. 19, with upper trace at 250 volts/cm and lower trace at 50 gauss/cm. The phase of the reflected fields is the same as for a nonconducting boundary, indicating that the copper wall is isolated from the plasma.

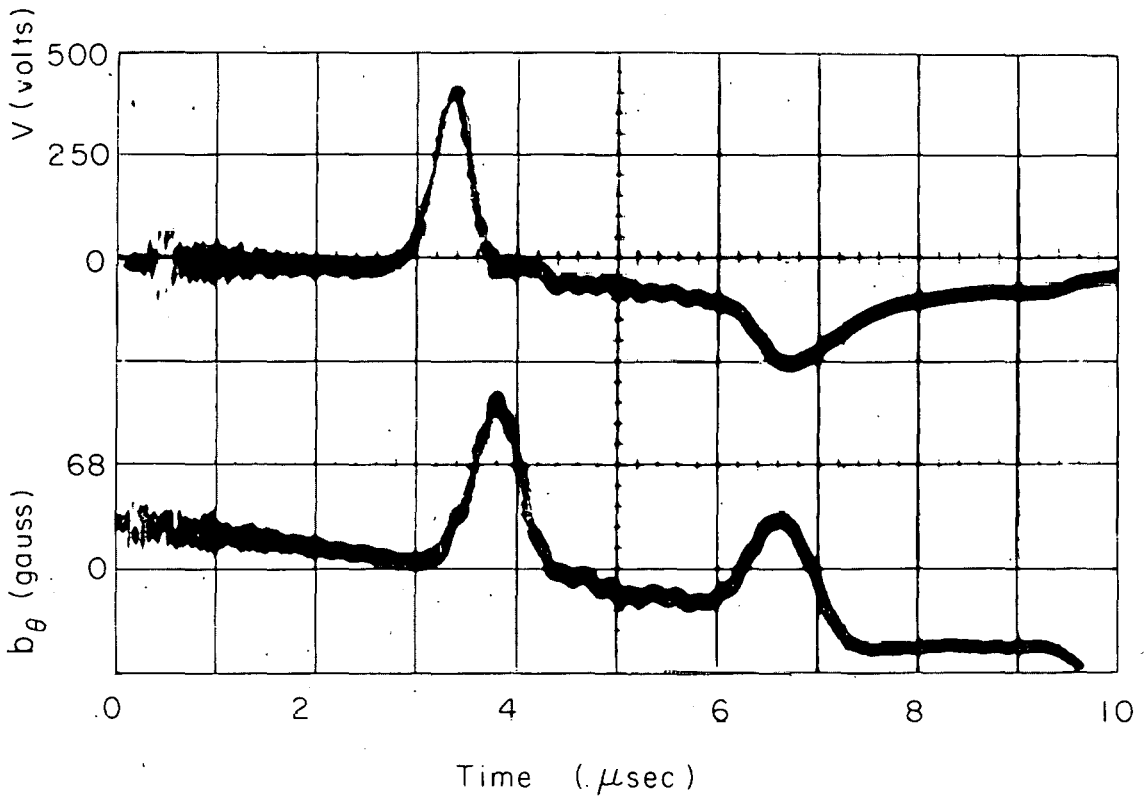

ZN-2620

Fig. 21. Oscillogram showing reflection from a copper plate with ionizing current still flowing to the plate. Traces are as in Fig. 19, with upper trace at 250 volts/cm and lower trace at 68 gauss/cm. The electric field has reflected out of phase, and the magnetic field in phase, in agreement with theory for a conducting boundary.

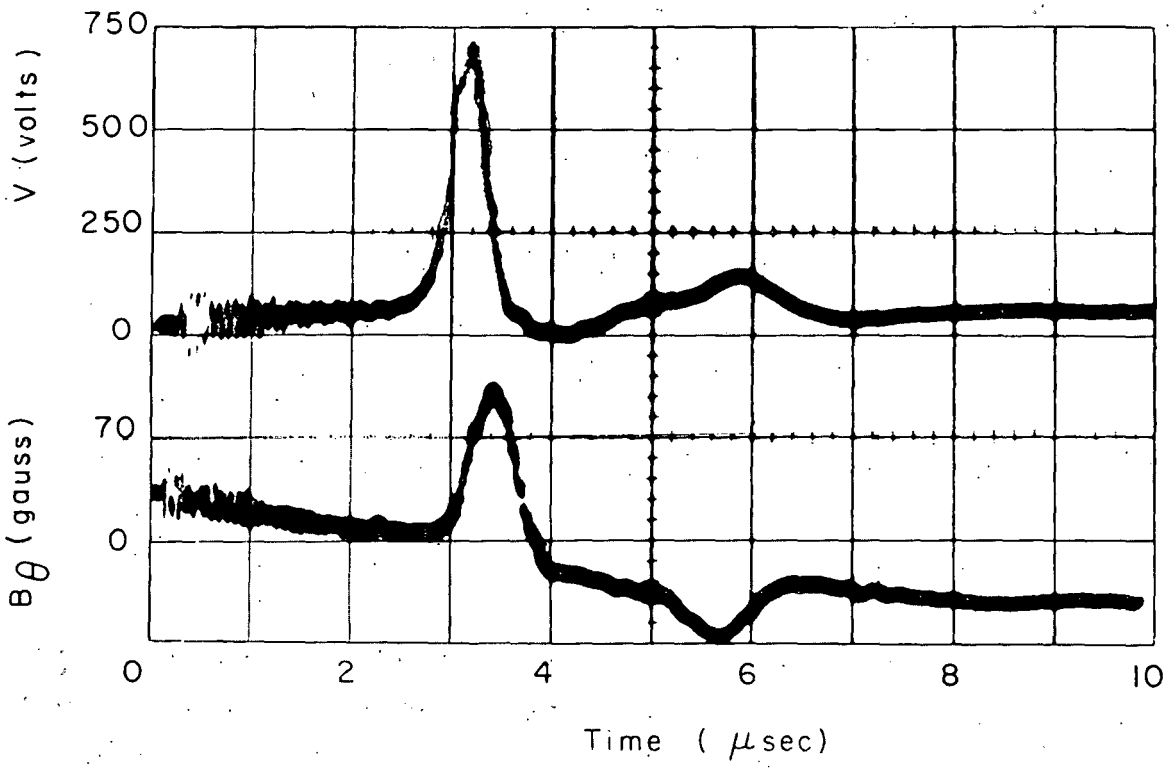

ZN-2621

Fig. 22. Oscillogram showing reflection from an interface between plasma and neutral gas. Upper trace is voltage on end electrode at 250 volts/cm, and lower trace is magnetic field at 70 gauss/cm. The phases indicate a nonconducting boundary at reflection. The small amplitude of the reflected signal indicates a lossy reflection.

obtained from measurements made while the tube was full of plasma, one calculates that the reflection occurred from a point 68 cm from the driving end, in reasonable agreement with the expected continued motion of the gasdynamic shock. At the same time, probes at the receiving end of the tube detected no wave magnetic field, as expected.

The observation of reflection of a hydromagnetic wave from an interface between plasma and an un-ionized gas may be compared with the recent observation of a similar type reflection occurring to a wave induced in the ionosphere which followed along the magnetic field lines of the earth's field, and was observed to reflect from the discontinuity between the ionosphere and the atmosphere.[29]

D. Radial Distribution of b_θ Field

The radial distribution of the azimuthal magnetic field b_θ associated with the wave has been measured with magnetic probes. Six probes were used, placed near the receiving end insulator at various radii. The result of this measurement is displayed in Fig. 23. The upper solid curve results from experimental data for a wave induced 20 μsec after the ionizing current was crowbarred (The lower solid curve will be discussed).

The observed b_θ becomes zero at the tube wall. Reference to Eqs. (2.43) and (2.46) shows that for any given mode, b_θ and j_r have the same radial dependence. We are here observing essentially only the lowest mode, therefore the observation indicates that no radial currents flow to the tube wall, as was previously noted in the section on theory. This observation was found to be true independently by looking for wall currents with the radial current probes (Fig. 5). At first glance the result is surprising, since the conductivity of the copper is much higher than that of the plasma, and since the method of inducing the wave requires a current to flow to the wall. However, for the same reasons discussed in the section on reflections from a copper boundary (IV-C), the electrical conductivity in the plasma adjacent to the wall

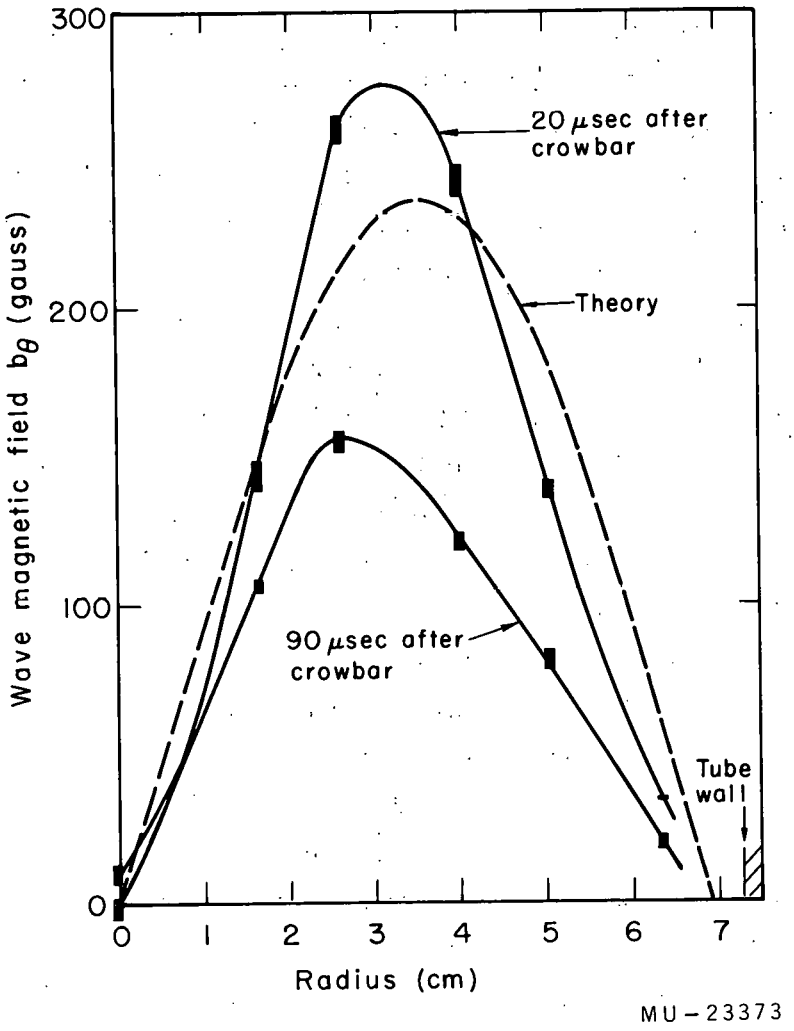

Fig. 23. The radial distribution of the wave magnetic field b_θ, measured near the receiving end of the tube after the wave has made one transit. The upper dashed curve is the theoretical distribution calculated from Table II for a wave induced 20 μsec after crowbar. The upper solid curve is the measured distribution for a wave induced 20 μsec after crowbar, and the lower solid curve is the measured distribution for a wave induced 90 μsec after crowbar.

may be low, isolating the plasma from the wall. The same distributions of b_θ were observed with either polarity of driving current, so this effect does not seem to be associated with the well known anode sheath which is sometimes observed in discharges where the current flow to a boundary surface is perpendicular to the static magnetic field.

The calculations of Table II lead to the theoretical prediction for $b_\theta(r)$ which is shown as a dashed line in Fig. 23. The zero of the Bessel functions was taken to be 4 mm inside the physical boundary, to better match the experimental data: this distance may be interpreted as roughly indicating the thickness of the non-conducting layer of gas. The measured value of V_0, used to determine the scale of the theoretical curve, was subject to an error here of ±10%. The agreement of the observed wave amplitude with that predicted on the basis of knowledge of the peak voltage applied to the driving end is remarkably good. It indicates that it has been possible to account for the energy flow from the external circuit into wave energy and the subsequent damping of this wave as it traveled through the tube.

The radial distribution of the wave magnetic field b_θ was also measured for a wave which had reflected from the receiving end of the tube and then from the driving end, i.e., the wave made three transits of the tube. The result is displayed in Fig. 24, where the dashed curve represents the lowest T type mode. The exact shape of the theoretical distribution is not reproduced in the measurements for either the single transit or the three-transit wave. The most likely explanation for this observation is that the plasma temperature may be somewhat non-uniform.

The lower solid curve of Fig. 23 is the distribution of b_θ measured for a wave that was induced 90 μsec after the ionizing current was crowbarred (For the previous discussion the waves were induced 20 μsec after crowbar). In this case, the peak of the distribution is shifted toward the axis of the tube. This observation would be consistent with the assumption that the decaying plasma has a radial temperature gradient with the warmest plasma (which would produce less wave attenuation) near the center of the tube.

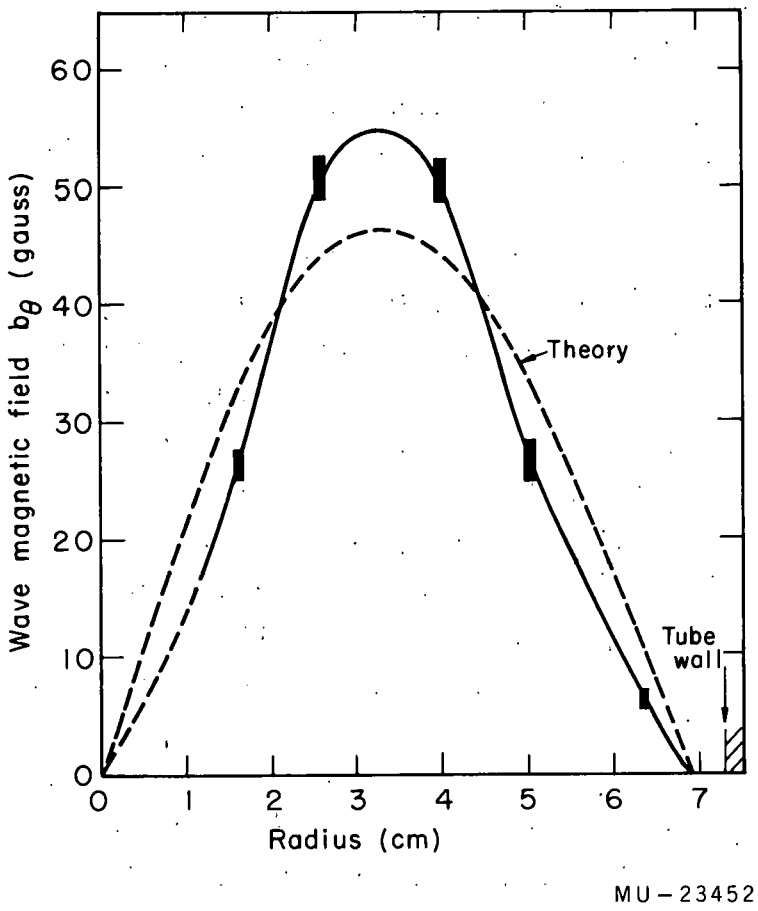

Fig. 24. The radial distribution of the wave magnetic field b_θ, measured near the receiving end of the tube after the wave has made three transits of the tube (i.e., two reflections). The dashed curve is the theoretical distribution for the lowest mode, from the information in Table II.

E. Auxiliary Checks

The theoretical analysis postulates azimuthally symmetrical waves. The driving electrode system has this property, and the cylinder was carefully aligned with the axial magnetic field, using a method which has been previously reported.[26] The symmetry of the wave was measured by a set of four magnetic field probes, placed 90 deg apart on the same base circle and oriented to pick up the θ component of the wave field. A random shot-to-shot variation of 20% was observed in individual probe signals, but the average of several shots gave azimuthal symmetry to within a few percent.

In order to justify the assumption that we are actually measuring the properties of the T-type waves, we measured the radial and axial components of the wave magnetic field. According to the theory of Sec. II, these components are of order $\Omega\beta^2$ if we excite only the T-type wave. For the highest frequencies of interest, ω is approx 10^7 sec^{-1} and so $\Omega\beta^2$ is approx 10^{-2}, and the amplitude of b_r should be negligibly small. It was possible to show experimentally only that b_r is less than 10% of the amplitude of b_θ, (probably due to the presence of $m \neq 0$ modes) so the assumption that we are working with T-type waves seems to be justified.

The maximum perturbation magnetic field produced in the plasma in these experiments was of the order of 500 gauss, which is only 3% of the static axial field, indicating that a small amplitude analysis should be valid. To check this, a measurement of wave velocity was made, varying the magnitude of the initial perturbation. The initial charge on the wave generation capacitor was varied from 4 to 16 kv, without noticeably affecting wave velocity. The results of this measurement appear in Fig. 25.

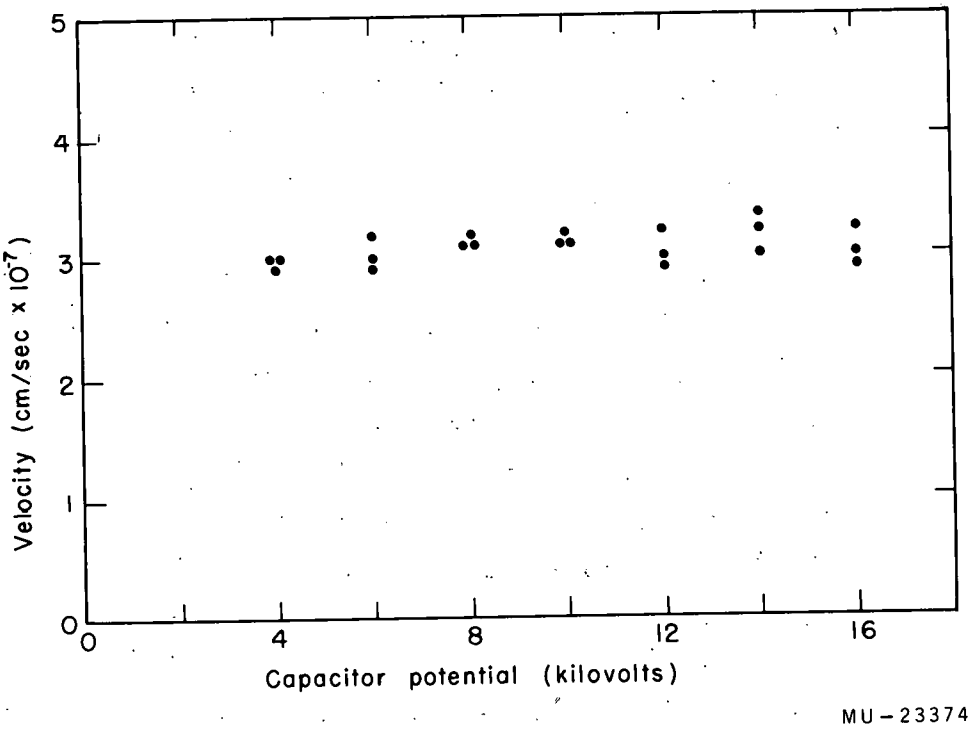

Fig. 25. Measured wave velocity vs potential on wave generation capacitor.

V. DISCUSSION

We have observed a number of the phenomena associated with hydromagnetic waves and, where comparisons with theory are possible, have found generally good agreement. The limitations on the precision of measurements stem almost entirely from the dual difficulties of producing a uniform, clean plasma and of measuring its properties. While it cannot be said that the plasma with which we work is absolutely pure or uniform, it is at least close enough to these ideals to allow comparisons with theory to within about 20%. To this level of accuracy, we found good agreement with theory in all our measurements.

Determinations of the plasma density and temperature in the ranges of parameters used in this experiment are not easily made. It seems from our work that Alfvén waves may well be used in future experments as fast, nonperturbing probes to measure these important quantities. The particle density is simply related to the wave velocity, which is easily measured. In any specific case, the coupling between neutral particles and ions will have to be considered, in order to make clear just what density is being measured, but this should present no great problem.

Temperature determination is accomplished by measuring the wave attenuation, which gives directly the resistivity of the plasma. The temperature is then calculated from one of the theoretical formulae for resistivity (see e.g., Spitzer,[11] p. 84). In the case where the resistivity is very low, the waves will propagate along the magnetic flux tube in which they are initially induced, without appreciable spreading, thus offering the possibility of making space resolved measurements.[31]

Several further experiments are suggested by this work. The phenomenon of the switch-on ionization wave which is used to produce the plasma is not at all well understood, and much further experimental and theoretical work is needed. Since the plasma made in this manner seems to be a convenient one with which to work, a better understanding of the ionization process may be of considerable practical interest.

It has been pointed out by Gajewski[32] that the cylindrically symmetric mode investigated in this work does not represent the "lowest" mode, since for the observed boundary conditions there exists an $m = 1$ mode for which k_c is smaller than the k_{c1} of this paper, which should lead to considerably lower dissipation for the $m = 1$ mode. Some indication of the existence of this mode has been noted, at a time when an asymmetric drive was being tried, but no careful measurements have been made.

The cross section for charge-exchange collisions between protons and atomic hydrogen occurs in the expression for attenuation due to the presence of neutral atoms. It may be possible to measure this cross section by measuring the damping of waves in some region where neutral damping is dominant over resistive damping. Since no experimental determination of the cross section has been made for energies below 100 ev, this would be of basic interest.

Finally, the need to find the temperature of the plasma has led to a proposal to measure the temperature by observation of the recombination radiation of the Balmer continuum. This proposal is being investigated at this laboratory.

APPENDICES

A. Effect of Neutral Particles

The effects produced by neutral particles in a nearly fully-ionized plasma have been discussed in detail by Lehnert.[33] For the purposes of this work it will only be necessary to take into account the effective frictional force between ions and neutrals, considering the two species as interpenetrating fluids. This force is expressed by the last term of Eq. (2.8), in which the rate of transfer of momentum from ions to neutrals is assumed to be proportional to the difference between ion and neutral average velocities. The equation for neutrals corresponding to Eqs. (2.1) and (2.2) for ions and electrons is

$$n_n m_n \frac{\partial \underset{\sim}{v}_n}{\partial t} = \underset{\sim}{P}^{ne} + \underset{\sim}{P}^{ni}, \qquad (A.1)$$

where n_n is the number density of neutral particles, and m_n is their mass.

We will now derive an expression for $\underset{\sim}{P}^{ni}$, the momentum transfer between neutrals and ions. $\underset{\sim}{P}^{ne}$ is assumed negligible since neutral-electron momentum transfer is relatively slow.

If z is the number of collisions per unit volume per second between neutrals and ions, then

$$z = n_n \nu_{ni}, \qquad (A.2)$$

where n_n is the number density of neutrals and ν_{ni} is the frequency of collisions of a neutral with ions. We now assume that in a collision the neutral loses all "memory" of the wave motion it may have carried prior to the collision. The wave momentum gained by a neutral per collision is proportional to the relative average velocity of ions and neutrals, and is $m(\underset{\sim}{v}_i - \underset{\sim}{v}_n)$ (the charge-exchange cross section is much larger than any other ion-neutral cross section at the energies of interest here, so we consider only charge-exchange collisions. Such

collisions are always in effect head-on collisions, in the center-of-mass system).

We then have

$$\underset{\sim}{P}^{ni} = m(\underset{\sim}{v}_i - \underset{\sim}{v}_n)\, n_n\, \nu_{ni} = mn_n \frac{\partial \underset{\sim}{v}_n}{\partial t} \quad . \tag{A.3}$$

Assuming harmonic time dependence and solving for $\underset{\sim}{v}_n$ gives

$$\underset{\sim}{v}_n = \frac{1}{1 - i\tau}\, \underset{\sim}{v}_i \tag{A.4}$$

where τ is defined as ω/ν_{ni}. If τ is small, the two fluids are closely coupled and move practically together, with a phase lag given by $\tan^{-1}\tau$. In the work quoted here, $\omega \approx 4\times10^{6}\ \text{sec}^{-1}$ and $\nu_{ni} \approx 4\times10^{7}\ \text{sec}^{-1}$, so τ is about 0.1, and may be considered small as a first approximation. We define ρ_n equal to $m_n n_n$. Then using Eq. (A.4) to eliminate $\underset{\sim}{v}_n$ from (A.3) gives

$$\underset{\sim}{P}^{ni} = -i\omega \rho_n \frac{1}{1 - i\tau}\, \underset{\sim}{v}_i \ , \tag{A.5}$$

which is the expression used in deriving Eq. (2.13).

B. Derivation of Vector Wave Equation

We seek to derive an equation for the perturbed magnetic field $\underset{\sim}{b}$ from the set of Eqs. (2.9), (2.10), (2.11), and (2.12). We start by solving Eq. (2.12) for $\underset{\sim}{v}_i$

$$\underset{\sim}{v}_i = \frac{1}{\omega \rho_1}\, \underset{\sim}{j} \times \underset{\sim}{B}_0 \tag{B.1}$$

This is now substituted into Eq. (2.9) to give

$$\underset{\sim}{E} + \frac{i}{\omega\rho_1}(\underset{\sim}{j} \times \underset{\sim}{B}_0) \times \underset{\sim}{B}_0 = \underset{\sim}{\eta} \cdot \underset{\sim}{j} + \frac{1}{cn}\, \underset{\sim}{j} \times \underset{\sim}{B}_0 \qquad (B.2)$$

We now use Eq. (2.10) to eliminate $\underset{\sim}{j}$ from Eq. (B.2)

$$\underset{\sim}{E} + \frac{i}{\omega \rho_1 \mu_0}\left[(\nabla \times \underset{\sim}{b}) \times \underset{\sim}{B}_0\right] \times \underset{\sim}{B}_0 = \frac{1}{\mu_0}\, \underset{\sim}{\eta} \cdot \nabla \times \underset{\sim}{b} + \frac{1}{\mu_0 en}(\nabla \times \underset{\sim}{b}) \times \underset{\sim}{B}_0 \,. \qquad (B.3)$$

Finally we take the curl of this equation and substitute Eq. (2.11), curl $\underset{\sim}{E} = i\omega \underset{\sim}{b}$, to get

$$\underset{\sim}{b} = -\frac{B_0^{\,2}}{\omega^2 \mu_0 \rho_1} \nabla \times \left\{\left[(\nabla \times \underset{\sim}{b}) \times \hat{z}\right] \times \hat{z}\right\} + \frac{1}{i\omega\mu_0} \nabla \times (\underset{\sim}{\eta} \cdot \nabla \times \underset{\sim}{b})$$
$$+ \frac{B_0}{i\omega\mu_0 en} \nabla \times \left[(\nabla \times \underset{\sim}{b}) \times \hat{z}\right] \qquad (B.4)$$

where $\hat{z} = \underset{\sim}{B}_0 / B_0$.

Introducing $V^2 \equiv B_0^{\,2}/\mu_0\rho_1$ and $\omega_{ci} \equiv eB_0/m_i$ gives:

$$\underset{\sim}{b} = -\frac{V^2}{\omega^2} \nabla \times \left\{\left[(\nabla \times \underset{\sim}{b}) \times \hat{z}\right] \times \hat{z}\right\} - i\,\frac{1}{\omega\mu_0} \nabla \times (\underset{\sim}{\eta} \cdot \nabla \times \underset{\sim}{b})$$
$$- i\,\frac{\rho_1}{nm_i}\,\frac{V^2}{\omega\omega_{ci}} \nabla \times \left\{\left[\nabla \times \underset{\sim}{b}\right] \times \hat{z}\right\} . \qquad (B.5)$$

In a cartesian system the ith component of $\underset{\sim}{b}$ may be written

$$b_i = -\frac{V^2}{\omega^2}\left[\epsilon_{ijk}\frac{\partial}{\partial x_j}\,\epsilon_{klm}\,\hat{z}_m\epsilon_{lno}\,\hat{z}_o\,\epsilon_{npr}\frac{\partial}{\partial x_p}\,b_r\right] - i\frac{1}{\omega\mu_0}\left[\nabla\times(\underset{\sim}{\eta}\cdot\nabla\times\underset{\sim}{b})\right]_i$$

$$- i\,\frac{\rho_1}{nm_i}\frac{V^2}{\omega\omega_{ci}}\left[\epsilon_{ijk}\,\frac{\partial}{\partial x_j}\,\epsilon_{klm}\,\hat{z}_m\,\epsilon_{lop}\,\frac{\partial}{\partial x_o}\,b_p\right]. \qquad (B.6)$$

Since $\epsilon_{ijk}\,\epsilon_{lmk} = \delta_{il}\,\delta_{jm} - \delta_{im}\,\delta_{jl}$, we have

$$b_i = -\frac{V^2}{\omega^2}\left[\hat{z}_m\hat{z}_o(\delta_{il}\delta_{jm} - \delta_{im}\delta_{jl})(\delta_{op}\delta_{lr} - \delta_{or}\,\delta_{lp})\,\frac{\partial^2 b_r}{\partial x_j\,\partial x_p}\right]$$

$$-i\frac{1}{\omega\mu_0}\left[\nabla\times(\underset{\sim}{\eta}\cdot\nabla\times\underset{\sim}{b})\right]_i - i\frac{\rho_1 V^2}{nm_i\omega\omega_{ci}}\left[\epsilon_{ijk}\hat{z}_m(\delta_{mo}\delta_{kp} - \delta_{mp}\delta_{ko})\,\frac{\partial^2 b_p}{\partial x_j\,\partial x_o}\right]. \qquad (B.7)$$

Noting that $\hat{z}_i$ is the z direction, and going back to vector notation we get

$$\frac{\omega^2}{V^2}\,\underset{\sim}{b} = -\frac{\partial^2}{\partial z^2}\underset{\sim}{b} - \nabla^2 b_z\hat{z} + \nabla\frac{\partial b_z}{\partial z} - i\,\frac{1}{\omega\mu_0}\,\nabla\times(\underset{\sim}{\eta}\cdot\nabla\times\underset{\sim}{b}) - i\Omega\,\nabla\times\frac{\partial\underset{\sim}{b}}{\partial z}\,,$$

where we have introduced $\Omega \equiv \dfrac{\rho_1}{nm_i}\,\dfrac{\omega}{\omega_{ci}}$ . . . . . (2.14)

C. Cooling of Plasma by Thermal Conduction to the Wall

We consider the rate of heat transfer in the radial direction in a cylindrical plasma, due to thermal conductivity. Particle diffusion effects are ignored in this calculation, as is the effect of neutral particles. The conservation equation for thermal energy, assuming no sources or sinks, is

$$\frac{\partial W}{\partial t} - \nabla \cdot \kappa \nabla T = 0, \tag{C.1}$$

where $W = 3nkT$ is the thermal energy density, n is the ion density and κ is the coefficient of thermal conduction for a fully ionized plasma which is, from Spitzer,[11]

$$\kappa = g\, T^{5/2} \quad \text{erg/sec deg cm}, \tag{C.2}$$

where g is a constant which for the experiment has the value $g \approx 7.4 \times 10^{-6}$ erg/sec deg $^{7/2}$ cm. Since the tube wall is an electrical conductor and during the time of interest is short circuited to a central electrode, it should not be possible for a radial electric field to exist, so the thermoelectric effect is ignored. If a radial field could exist, κ would be reduced by a factor 0.419.

Equation (C.1) becomes, upon substitution for W and κ,

$$h \frac{\partial T}{\partial t} - \nabla \cdot \left(T^{5/2} \nabla T \right) = 0, \tag{C.3}$$

where $h = 3 \frac{nk}{g}$

This equation is nonlinear, but separable. Set $T = \tau(t)\, R(r)$, and let λ^2 be the separation constant. Then we obtain

$$\frac{d\tau}{dt} + \frac{\lambda^2}{h} \tau^{7/2} = 0; \tag{C.4}$$

$$\nabla^2 R + \frac{5}{2} R^{-1} (\nabla R)^2 + \lambda^2 R^{-3/2} = 0. \qquad (C.5)$$

The equation for the time variation is easily integrated and yields

$$\tau = \left[\frac{5}{2} \frac{\lambda^2}{h} t + \frac{1}{T_o}^{5/2} \right]^{-2/5} \qquad (C.6)$$

where T_o is the initial temperature at $r = 0$ and $t = 0$. A characteristic decay time is given by

$$t_o = \frac{h}{\lambda^2 T_o^{5/2}}, \qquad (C.7)$$

and is the time for the temperature to drop to $0.758\ T_o$.

To treat the R equation, we first assume cylindrical symmetry and negligible z variation of temperature (long cylinder approximation). Then $\frac{\partial}{\partial \theta} = \frac{\partial}{\partial z} = 0$.
In cylindrical coordinates, Eq. (C.5) becomes

$$\frac{d^2R}{dr^2} + \frac{1}{r} \frac{dR}{dr} + \frac{5}{2} \frac{1}{R} \left(\frac{dR}{dr} \right)^2 + \lambda^2 \frac{1}{R^{3/2}} = 0. \qquad (C.8)$$

We now make the following changes of variables:

$$R = \left(\frac{7}{2} \lambda^2 \gamma^2 \right)^{2/5} Z^{2/7}; \qquad (C.9)$$

$$r = \gamma s. \qquad (C.10)$$

The change of Eq. (C.10) is made for convenience later in scaling. With these substitutions, Eq. (C.8) becomes

$$\frac{d^2Z}{ds^2} + \frac{1}{s} \frac{dZ}{ds} + Z^{2/7} = 0 \qquad (C.11)$$

A solution to this equation can be found graphically, which serves to determine λ^2 and hence the characteristic decay time. A simple and very rough approach is to notice that the solutions to the two equations obtained by replacing the exponent $2/7$ in Eq. (C.11) by 0 or 1 are respectively $Z = 1 - s^2/4$ and $Z = J_o(s)$, where J_o is the zero order Bessel function. A plot of these two solutions out to the first zero of Z reveals that they are very similar (Fig. 26), and since they must bracket the solution to Eq. (C.11), we obtain immediately the approximate value $s \approx 2.1$ at the first zero of z. The physical boundary condition is assumed to be $T = 0$ at $r = 7.3$ cm, so we obtain from Eq. (C.10) $\gamma = 7.3/2.1 = 3.48$. Since the temperature at $r = 0$ has already been specified in τ, we must have $R(0) = 1$. Then Eq. (C.9) serves to determine λ^2, which is equal to 2.3×10^{-2} cm. The shape of the temperature distribution is obtained from the graphical solution for Z and Eq. (C.9), and is shown in Fig. 26. For this solution, the characteristic time from Eq. (C.7) is $t_o = 320$ μsec.

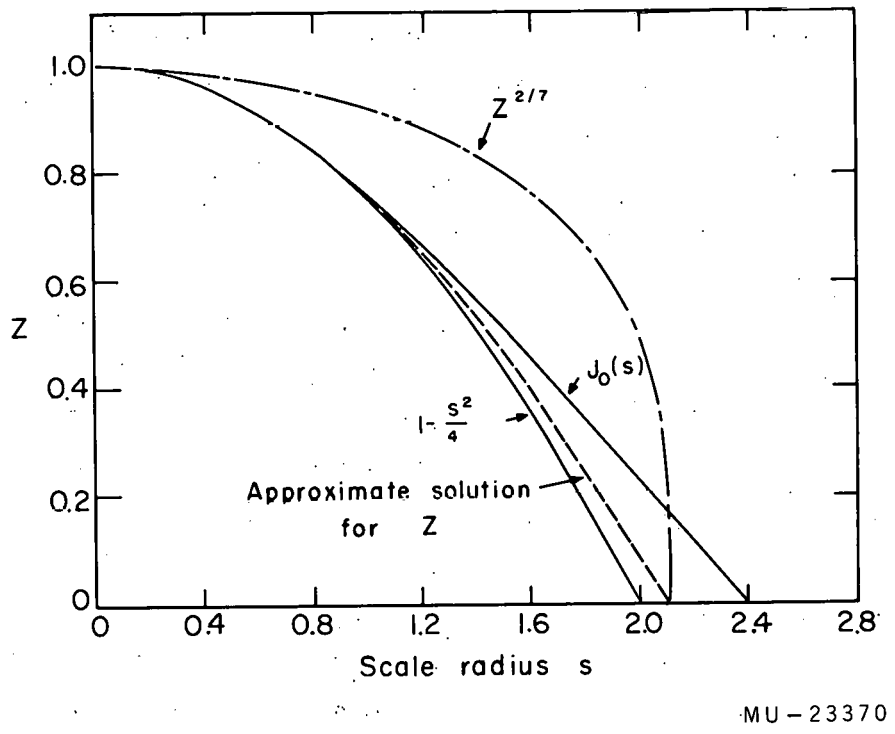

Fig. 26. Approximate solution to Eq. (C. 11). The upper dashed curve is the similarity solution for the radial dependence of temperature in the tube.

D. Review of Theoretical Literature Relating to Hydromagnetic Waves in Waveguides

The problem of hydromagnetic waves is a waveguide with a magnetic field directed along the axis of the guide has been treated by a number of authors. These papers will be briefly discussed here, mostly with regard to their respective limits of validity and their applicability in various extreme cases. For consistency the terminology of Gajewski will be used to refer to the various types of waves, because the designation of different wave types is by no means uniform among these authors. Since the work of Gajewski will be used as a frame within which the other work will be examined, we begin with a review of the results of his work.

Gajewski begins with the linearized equations of magnetohydrodynamics, as they appear in Eqs. (2.8) through (2.11) of this paper, with the exception that dissipative effects are ignored ($\gamma = \eta = 0$) and the $\underset{\sim}{j} \times \underset{\sim}{B}_0$ term of Eq. (2.9) is neglected. His results are applicable to waveguides of arbitrary cross section, and he gives some specific results for guides of circular cross section. He finds four types of waves. The first is a purely longitudinal wave which travels at sound speed and is identical to the principal wave of an acoustic guide, and is termed the L type wave. A second type is purely transverse, travels without dispersion at the Alfvén speed, and is called a T type wave. This is the type experimentally investigated in this paper. The third and fourth types involve both transverse and longitudinal displacements and are termed TL types. These last two waves are examined in detail for the case where sound speed V_s greatly exceeds the Alfvén speed V. Under these conditions, one wave travels at nearly the Alfvén speed and is called a TLM (magnetohydrodynamic) type, and one travels at nearly sound speed and is called a TLA (acoustic) type. Unfortunately, the notation is inconsistent for the opposite case of $V \gg V_s$, for in this case the TLA type travels at nearly the Alfvén speed and the TLM type travels at sound speed.

The earliest work in this field was done by Lundquist.[5] His work is a simplified theory giving only the m = 0, T type wave, with the inclusion of finite conductivity. This theory is used in his paper for a comparison with his experimental results in mercury.

In 1954 this work was extended by Lehnert,[6] both experimentally and theoretically. The theory used by Lehnert was similar to that of Lundquist, treating only the m = 0, T type wave.

The first author to treat the general problem of hydromagnetic waves in a cylindrical geometry was Baños.[34] He starts with a general set of equations retaining not only a finite conductivity, but the displacement current term in the curl $\underset{\sim}{B}$ equation. These inclusions allow him to examine the behavior of the wave types in the limiting cases of low static magnetic field, where the wave goes over to an ordinary electromagnetic wave, and of finite conductivity, in which case the waves are damped by ohmic losses within the fluid. Baños does not examine in detail all the wave types, and finds the T type and the extremes of the TLA wave for $V_s \gg V$ and $V_s \ll V$.

Newcomb[14] looks specifically at the case of a waveguide of circular cross section with electrically conducting walls and with $V \gg V_s$. He starts with the same set of equations as Gajewski, and finds the T and TLA waves. Then, treating the terms individually as perturbations, he finds the effect on these waves of finite conductivity, pressure gradients within the plasma, and of the term $\frac{1}{en}\ \underset{\sim}{j} \times \underset{\sim}{B}$ which appears in Ohm's law. The conductivity term leads to damping constants for the two types of waves. With the inclusion of pressure gradients, he finds the TLM type wave, and the last term leads to a rotation of the plane of polarization of the two TL waves.

Lehnert's work[33] is very general in leading up to a vector wave equation for $\underset{\sim}{b}$, the wave magnetic field. It includes the effects of neutral atoms within the plasma, finite conductivity and displacement currents. However, in applying this equation, he allows some sweeping approximations to be made which reduce the equation to one containing only the m = 0, T type wave. From our experimental point of view this is still very interesting though, since the effects of neutral atoms are still included.

This effect had not been taken into account by other workers.

Finally, Schmoys and Mishkin[35] have recently treated the problem of a guide of arbitrary cross section, containing a plasma of finite conductivity and including the effect of displacement currents. Since they do not include pressure effects, they only find the T type wave and the $V \gg V_s$ limit of the TLA type.

An intersting case occurs when the wave frequency approaches the ion cyclotron frequency. The T-type wave shows a resonance effect at this frequency, where the attenuation becomes very high and the wave velocity goes to zero. This problem has been thoroughly examined by Stix,[16] in connection with is proposals to use this resonance as a means for plasma heating. This work has recently been extended by Bernstein and Trehan.[36] They develop a dispersion relation for the T-type wave (their Eq. IV-25) which is identical to the zero resistivity limit (Eq. 2.37) of Eq. (2.34) of this thesis.

The terminology used by various authors to designate these waves is presented in tabular form in Table III.

Table III

Comparisons of wave terminology of various authors

Gajewski[15]	Baños[34]	Newcomb[14]	Lehnert[33]	Schmoys & Mishkin[35]
L	---	---	---	---
T	Velocity mode	Principal mode	Torsional mode	TM mode
TLM ($V \gg V_s$)	in equations but not specifically named	Sound-like mode	---	---
TLM ($V \ll V_s$)	in equations but not specifically named	---	---	---
TLA ($V \ll V_s$)	Modified sound wave	---	---	---
TLA ($V \gg V_s$)	Modified Alfven wave	TE mode	---	TE mode

BIBLIOGRAPHY

Akhiezer, A. I., G. J. A. Lubarski, and R. V. Polovin, Simple Waves and Shock Waves in Magnetohydrodynamics, in Proceedings of the Second United Nations International Conference on the Peaceful Uses of Atomic Energy (United Nations, Geneva, 1958), Vol. 31, p. 225.

Alfvén, H., A New Type of Wave Motion and Its Importance in Solar Physics, Acta Radiologica XXVII, 238 (1946).

Allis, W. P., Waves in a Plasma, in Proceedings of the Conference on Theoretical Aspects of Controlled Fusion Research (1959), p. 32.

Anderson, N. S., Longitudinal Magneto-Hydrodynamic Waves, J. Acoust. Soc. Am. 25, 529 (1952).

Auer, P. L., H. Hurwitz, and R. D. Miller, Collective Oscillations in a Cold Plasma, Phys. Fluids 1, 501 (1958).

Baños, A., and R. Vernon, Large Amplitude Waves in Collision-Free Plasma I, Nuovo cimento, Series X, 13, 269 (1960).

Blank, A. A., and H. Grad, Notes on Magnetohydrodynamics VI. -Fluid Magnetic Equations; General Properties, Institute of Mathematical Sciences Report NYO-6486 New York University, New York, 1958 (unpublished).

Braginskii, S. I., and A. P. Kazantsev, Magnetohydrodynamic Waves in a Rarified Plasma, in Plasma Physics and the Problems of Controlled Thermonuclear Reactions (Pergamon Press, Ltd., London, 1960) Vol. IV, p. 24.

Carim, G., Observations on Cylindrical Waves in Magnetohydrodynamics, R. C. Accad. Naz. Lincei 22, 482 (1957).

Chandrasekhar, S., A. N. Kaufman and K. M. Watson, Properties of an Ionized Gas of Low Density in a Magnetic Field, Part IV, Ann. Phys. 5, 1 (1958).

Chandrasekhar, S., Plasma Physics (University of Chicago Press, Chicago 1960).

Cole, J. D., Magnetohydrodynamic Waves, Office of Scientific Research Report AFOSR-TN-59-13, AD208 594, Baltimore, Maryland, 1959 (unpublished).

Covert, E. E., and K. Kerney, A Review of the Literature of Plasma Physics, MIT Naval Supersonic Laboratory Technical Report 373 (WADD Technical Report 59-486), July 1959 (unpublished).

Cowling, T. G., Magnetohydrodynamics, (Interscience Publishers, Inc., New York, 1957).

Cowling, T. G., Magnetohydrodynamic Oscillations of a Rotating Fluid Globe, Proc. Roy. Soc. (London) 233A, 319 (1955).

Dawson, J., and C. Oberman, Oscillations of a Finite Cold Plasma in a Strong Magnetic Field, Phys. Fluids 2, 103 (1958).

Delcroix, J. L., Introduction to the Theory of Ionized Gases (Interscience Publishers Inc. New York, 1960).

Dungey, J. W., Derivation of the Dispersion Equation for Alfvén Magneto-Hydrodynamic Waves from Bailey's Electromagnetic-Ionic Theory, Naturc 167, 1029 (1951).

Elsasser, W. M., The Hydromagnetic Equations, Phys. Rev. 79, 183, (1950).

Ferraro, V. C. A., Hydromagnetic Waves in a Rare Ionized Gas and Galactic Magnetic Fields, Proc. Roy. Soc. (London) 233A, 310 (1955).

------ General Theory of Plasma, Nuovo cimento Supp. 13, 9 (1959).

Gallet, R., Propagation and Production of Electromagnetic Waves in a Plasma, Nuovo cimento Supp. 13, 234 (1959).

Gershman, B. N., V. L. Ginzburg, N. G. Denisov, Propagation of Electromagnetic Waves in a Plasma, Soviet Phys-Uspekhi, 61, 561 (1957), U. S. Atomic Energy Commission Translation AEC tr-3493 (unpublished).

Gershman, B. N., Kinetic Theory of Magneto-Hydrodynamic Waves, Zhur. Eksp. Teoret. Fiz. 24, 453 (1953). AEC-tr-3371

Ginzburg, V. L., Magnetohydrodynamic Waves in Gases, Soviet Physics-JETP 21, 788 (1951).

Halbach, K., The Frequency Dependence of the Conductivity of a Uniform Plasma in a Uniform Magnetic Field and the Propagation of Electromagnetic Waves along Field Lines, Engineering Note UCID-755, Lawrence Radiation Laboratory, California, June 1959 (unpublished).

Halbach, K., Propagation of Electromagnetic Waves in a Plasma Perpendicular to a Magnetic Field, Engineering Note UCID-817, Lawrence Radiation Laboratory, California, July 1959 (unpublished).

Hide, R., Waves in a Heavy, Viscous, Incompressible, Electrically Conducting Fluid of a Variable Density, in the Presence of a Magnetic Field, Proc. Roy. Soc. (London) 233A, 376 (1955).

Hines, C. O., Magneto-Ionic Approach to Magnetohydrodynamic Waves, Generalized Magneto-hydrodynamic Formulae, Proc. Cambridge Phil. Soc. 49, Part 2, 299 (1953).

Kahalas, S. L., Magnetohydrodynamic Wave Propagation in the Ionosphere, Phys. Fluids 3, 372 (1960).

Kantor, M., Plasma Oscillations and Dispersion in the Presence of a Magnetic Field, Space Technology Laboratories Inc. Report PRL 6M-TR-0165-00526, El Segundo, California, November 1958 (unpublished).

Karplus, R., Radiation of Hydromagnetic Waves, Phys. Fluids 3, 800 (1960).

Kautzleben, H., Betrachtungen zur hydromagnetischen Theorie des Plasmas–Hydromagnetische Wellen, (Akademie-Verlag, Berlin, 1958).

Layzer, D., M. Krook, and D. H. Menzel, Torsional Oscillations and Solar Magnetic Fields, Proc. Roy. Soc. (London) 233A, 302 (1955).

Lehnert, B., Magnetohydrodynamic Waves under the Action of the Coriolis Force, Astrophys. J. 119, 647 (1954).

Lehnert, B., On the Behavior of an Electrically Conductive Liquid in a Magnetic Field, Arkiv. Fysik 5, No. 5 (1951).

------ Magnetohydrodynamic Waves in the Ionosphere and their Application to Giant Pulsations, Tellus 8, 241 (1956).

Linhart, J. G., Plasma Physics (North-Holland Publishing Co., Am-

sterdam; Interscience Publishers, Inc., New York, 1960).

Lundquist, S., Studies in Magnetohydrodynamics, Arkiv f. Fysik 5, 297 (1952).

Montgomery, D., Non-Linear Alfvén Waves in a Cold Ionized Gas, Phys. Fluids 2, 585 (1959).

Oster, L., Linearized Theory of Plasma Oscillations, Revs. Modern Phys. 32, 141 (1960).

Piddington, J. H., Hydromagnetic Waves in Ionized Gas, Monthly Not. Royal Astron. Soc. 115, 671 (1954).

------ The Motion of Ionized Gas in Combined Magnetic, Electric and Mechanical Fields of Force, Monthly Not. Royal Astron. Soc. 114, 651 (1954).

Reichel, P., Basic Notions of Relativistic Hydromagnetics, NYO-7697, 1958 (unpublished).

Richter, E., Fuer Theorie Magnetohydrodynamische Wellen, Z. Naturforsch. 11A, 251 (1956).

Roberts, P. H., On the Reflection and Refraction of Hydromagnetic Waves, Astrophys. J. 121, 720 (1955).

Schmoys, J., and E. Mishkin, On the Linear Behavior of Large-Amplitude Magnetohydrodynamic Waves, Phys. Fluids 3, 661 (1960).

Spitzer, L. Jr., Physics of Fully Ionized Gases, (Interscience Publishers, Inc., New York 1957).

Stepanov, K. N., Kinetic Theory of Magnetohydrodynamic Waves, Soviet Physics-JETP 34, 1292 (1958).

Sugiura, M., Some Evidence of Hydromagnetic Waves in the Earth's Magnetic Field, Phys. Rev. Letters 6, 255 (1961).

Van de Hulst, H. C., Problems of Cosmical Aereodynamics (Central Air Documents Office, Dayton 2, Ohio, 1951).

Lanier, S. F., R. L. Scott, and T. W. Scott, Controlled Thermonuclear Reactions-A Selective Bibliography, Rev. ed., TID-3072 (Rev. 1), USAEC Office of Technical Information Report, January 1961.

Scott, R. L., and S. F. Lanier, Controlled Thermonuclear Processes, USAEC Office of Technical Information Report, November 1960 (unpublished).

Spence, B. A., Bibliography on Magnetohydrodynamics, Plasma Physics, and Controlled Thermonuclear Processes, Avco-Everett Research Laboratory Report, AMP-36 October 1956.

Magneto-Fluid-Dynamics--Bibliography 1, NATO, Palais de Chaillot, Paris 16 (Pitman Press, Bath, England, 1960).

APPENDIX F

Plasma Boundary Condition*

We assume the plasma to be surrounded by a thin annular vacuum space of thickness ξ, with the plasma-vacuum boundary at $r_0 = b - \xi$. The vacuum space is bounded by a conducting wall at $r = b$. To obtain the conditions on the $_ik_c$, we match the tangential electric and magnetic fields in plasma to those in vacuum and put the appropriate conditions on the vacuum fields at the conducting wall.

The plasma fields are obtained from Eqs. (2.23), (2.18), and (2.9) through (2.12). We require the tangential components of $\underset{\sim}{b}$ and $\underset{\sim}{E}$ at $r = r_0$. To simplify the following expressions, we define the symbol [ ] such that

$$[\, Af(D_\perp, k_c)] \equiv \sum_{i=1,2} A_i f(_iD_\perp, {}_ik_c) . \tag{F1}$$

The fields at $r = r_0$ are then:

$$b_r = [AJ_1(k_c r_0)\,], \tag{F2}$$

$$b_\theta = \frac{i}{\Omega p^2}\,[(D_\perp - k_c^2)\,AJ_1(k_c r_0)], \tag{F3}$$

$$b_z = \frac{i}{p}\,[k_c AJ_0(k_c r_0)], \tag{F4}$$

$$E_\theta = -\frac{\omega}{p}\,[AJ_1(k_c r_0)\,], \tag{F5}$$

and

$$E_z = \frac{ia_\parallel V^2}{\Omega p^2 \omega}\,[k_c(D_\perp - k_c^2)AJ_0(k_c r_0)\,]. \tag{F6}$$

The vacuum solutions are well known: If we define

---

*The author is indebted to Dr. Klaus Halbach and Mr. Gary Pearson for valuable discussion regarding this condition.

$$\gamma^2 \equiv \frac{\omega^2}{c^2} - p^2 , \tag{F7}$$

$$S_1(\gamma r) \equiv C_1 J_1(\gamma r) + C_2 N_1(\gamma r) , \tag{F8}$$

and

$$T_1(\gamma r) \equiv G_1 J_1(\gamma r) + G_2 N_1(\gamma r), \tag{F9}$$

then at $r = r_0$ the vacuum fields are:

$$b_{\theta v}(r_0) = T_1(\gamma r_0), \tag{F10}$$

$$b_{zv}(r_0) = \frac{i\gamma}{p} S_0(\gamma r_0) , \tag{F11}$$

$$E_{\theta v}(r_0) = - \frac{\omega}{p} S_1(\gamma r_0) , \tag{F12}$$

and

$$E_{zv}(r_0) = \frac{ic^2\gamma}{\omega} T_0(\gamma r_0) . \tag{F13}$$

We now assume $\xi << b$, $\gamma\xi << 1$, and expand S_1, S_0, T_1, T_0 about b, noting that the boundary condition on E_{tan} at $r = b$ requires $S_1(\gamma b) = T_0(\gamma b) = 0$. The results are, to first order in ξ:

$$T_1(\gamma r_0) = (1 + \frac{\xi}{b}) T_1(\gamma b) , \tag{F14}$$

$$T_0(\gamma r_0) = \xi\gamma T_1(\gamma b), \tag{F15}$$

$$S_1(\gamma r_0) = - \xi\gamma S_0(\gamma b), \tag{F16}$$

and

$$S_0(\gamma r_0) = S_0(\gamma b) . \tag{F17}$$

Eqs. (F10), (F13), (F14), and (F15) show that $b_{\theta v}(r_0) \propto E_{zv}(r_0)$, and Eqs. (F11), (F12), (F16), and (F17) show that $b_{zv}(r_0) \propto E_{\theta v}(r_0)$. Since the plasma fields at the interface must match the vacuum fields, the above conditions give the following relations between b_θ and E_z and between b_z and E_θ in plasma, at $r = r_0$:

$$i\xi \left[(D_\perp - k_c^2)\, AJ_1(k_c r_0)\right] - \frac{a_\parallel V^2}{c^2 \gamma^2} \left(1 + \frac{\xi}{b}\right) \left[(k_c (D_\perp - k_c^2) AJ_0(k_c r_0)\right] = 0 \tag{F18}$$

$$-\xi \left[k_c\, AJ_0(k_c r_0)\right] - \left[AJ_1(k_c r_0)\right] = 0 . \tag{F19}$$

We consider the special case $(V^2/c^2)(k_c/\gamma^2)\, a_\parallel << \xi << \frac{1}{k_c}$, for which the second pair of terms of Eq. (F18) and the first pair of terms of Eq. (F19) are negligible. The first inequality requires essentially that the capacitive reactance of the vacuum layer be much greater than the resistance of an equally thick layer of plasma. Substituting from Eq. (F19) into Eq. (F18), we obtain

$$({}_1k_c^2 - {}_2k_c^2)\, A_1\, J_1\, ({}_1k_c r_0) = 0 \tag{F20}$$

and

$$({}_2k_c^2 - {}_1k_c^2)\, A_2\, J_1({}_2k_c r_0) = 0 . \tag{F21}$$

Equation (2.20) shows that, in general, ${}_1k_c$ is not equal to ${}_2k_c$, so we obtain as the solutions of interest

$$A_2 = 0;\ J_1({}_1k_c r_0) = 0 \tag{F22}$$

and

$$A_1 = 0;\ J_1({}_2k_c r_0) = 0 . \tag{F23}$$

These are equivalent, and show that only a single term (that is, i = 1 only) is needed to describe the wave field in Eq. (2.23). No additional information is obtained by considering the case ${}_1k_c = {}_2k_c$.

In the experiment, we have typically $(V^2/c^2)(k_c/\gamma^2)\, a_\parallel \approx 10^{-8}$ m and $1/k_c \approx 2\times10^{-2}$ m. The estimated value of ξ from experimental data is 4×10^{-3} m.

ACKNOWLEDGMENTS

The author wishes to express his deep appreciation to Dr. John Wilcox and Dr. Wulf Kunkel for the constant help and encouragement given by them in this work. The encouragement and contributions of Dr. C. M. Van Atta, Mr. William Baker and Dr. Forrest Boley are gratefully acknowledged. The invaluable assistance of Mr. William Cooper III and Mr. Peter Forman with the experimental work is also greatly appreciated.

This work was performed under the auspices of the U. S. Atomic Energy Commission.

REFERENCES

1. H. Alfvén, Ark. Mat., Astr. Fysik, 29B, 1 (1942); idem, Cosmical Electrodynamics (Clarendon Press, Oxford, 1950).
2. C. Walén, Ark. Mat., Astr. Fysik 30A No. 15 (1944); 31B, No. 3 (1944); 33A No. 18 (1946).
3. E. Astrom, Ark. Fys. 2, 443 (1950); Nature 165, 1019 (1950).
4. N. Herlofson, Nature 165, 1020 (1950).
5. S. Lundquist, Phys. Rev. 76, 1805 (1949); Nature 164, 145 (1949).
6. B. Lehnert, Phys. Rev. 94, 815 (1954).
7. W. H. Bostick and M. A. Levine, Phys. Rev. 87, 671 (1952).
8. T. K. Allen, W. R. Baker, R. V. Pyle, and J. M. Wilcox, Phys. Rev. Letters 2, 383 (1959).
9. D. F. Jephcott, Nature 183, 1652 (1959).
10. J. M. Wilcox, F. I. Boley, and A. W. DeSilva, Phys. Fluids 3, 15 (1960).
11. L. Spitzer, Jr., Physics of Fully Ionized Gases (Interscience Publishers Inc., New York, 1957).
12. It will be shown finally that the waves which are the subject of this experiment have approximately div $\underset{\sim}{v} = 0$, so pressure effects are absent to first order.
13. M. N. Rosenbluth and A. N. Kaufman, Phys. Rev. 109, 1 (1958).
14. W. A. Newcomb, in Magnetohydrodynamics (Stanford University Press, 1957), p. 109.
15. R. Gajewski, Phys. Fluids 2, 633 (1959).
16. T. H. Stix, Phys. Rev. 106, 1146 (1957).
17. G. N. Watson, A Treatise on the Theory of Bessel Functions, 2nd ed. (Cambridge University Press, New York).
18. R. W. Gould, Excitation of Alfvén Waves, Space Technology Laboratories Inc. Report STL/TR/60-000-09143 (May 24 1960).
19. See, e.g., N. H. Kemp and H. E. Petschek, Phys. Fluids 2, 599 (1959).

19a. O. A. Anderson, W. R. Baker, A. Bratenahl, H. P. Furth and W. B. Kunkel, J. Appl. Phys. 30, 188 (1959).

20. W. S. Cooper III, A. W. DeSilva, and J. M. Wilcox, Ion Density Measurements in a Decaying Hydrogen Plasma, Lawrence Radiation Laboratory Report UCRL-9509, March 1961.

21. J. Holtsmark, Ann. Physik 58, 577 (1919).

22. H. R. Griem, A. C. Kolb, and K. Y. Shen, Phys. Rev. 116, 4 (1959); idem, NRL Report 5455 (1960).

23. R. A. Gross and W. B. Kunkel, The Magnetic "Switch-On" Ionizing Wave, Lawrence Radiation Laboratory Report UCRL-9612, June 1961.

24. W. R. Baker, A. Bratenahl, A. W. DeSilva, and W. B. Kunkel, Proceedings of the 4th International Conference on Ionization Phenomena in Gases (North-Holland Publishing Co., Amsterdam, 1960) p. 1171.

24a. T. G. Northrup, in Controlled Thermonuclear Research Quarterly Report, Lawrence Radiation Laboratory Report UCRL-9598, March 1961.

25. W. L. Fite, R. T. Brackman and W. R. Snow, Phys. Rev. 112, 1161 (1958).

26. A Dalgarno and H. N. Yadav, Proc. Phys. Soc. (London) A66, 173 (1953).

27. R. Gajewski, and O. K. Mawardi, Phys. Fluids 3, 820 (1960).

28. Reflection of plasma Alfvén waves has been observed independently by S. Nagao and T. Sato, Tohoku University, Sendai, Japan (private communication).

29. H. A. Bomke, W. J. Ramm, S. Goldblatt, V. Klemas, Nature 185, 299 (1960).

30. A. W. DeSilva, and J. M. Wilcox, Rev. Sci. Instr. 31, 455 (1960).

31. H. Grad, in The Magnetohydrodynamics of Conducting Fluids, Stanford University Press, Stanford, California, 1959.

32. R. Gajewski, (private communication). Case Institute of Technology, Cleveland, Ohio.

33. B. Lehnert, Nuovo cimento Suppl. 13, No. 1 (1959), p. 59.
34. A. Baños, Proc. Roy. Soc. (London) A233, 350 (1955); Phys. Rev. 97, 1435 (1955).
35. J. Schmoys and E. Mishkin, Phys. Fluids 3, 473 (1960).
36. I. B. Bernstein and S. K. Trehan, Nuclear Fusion 1, 3 (1960).